Taylor & Francis
Taylor & Francis Group

The missing half of the subduction factory: shipboard results from the Izu rear arc, IODP Expedition 350

Cathy J. Busby[a], Yoshihiko Tamura[b], Peter Blum[c], Gilles Guèrin[d], Graham D. M. Andrews[e], Abigail K. Barker[f], Julien L. R. Berger[g], Everton M. Bongiolo[h], Manuela Bordiga[i], Susan M. DeBari[j], James B. Gill[k], Cedric Hamelin[l], Jihui Jia[m], Eleanor H. John[n], Ann-Sophie Jonas[o], Martin Jutzeler[p], Myriam A. C. Kars[q], Zachary A. Kita[r], Kevin Konrad[s], Susan H. Mahony[t], Michelangelo Martini[u], Takashi Miyazaki[b], Robert J. Musgrave[v], Debora B. Nascimento[h], Alexander R. L. Nichols[w], Julia M. Ribeiro[x], Tomoki Sato[b], Julie C. Schindlbeck[y], Axel K. Schmitt[z], Susanne M. Straub[aa], Maryline J. Mleneck-Vautravers[ab] and Alexandra Yang Yang[ac]

[a]Department of Earth and Planetary Sciences, University of California Davis, Davis, CA, USA; [b]Research and Development Center for Ocean Drilling Science, Japan Agency for Marine-Earth Science and Technology (JAMSTEC), Yokosuka, Japan; [c]International Ocean Discovery Program, Texas A&M University, College Station, TX, USA; [d]Lamont-Doherty Earth Observatory of Columbia University, Palisades, NY, USA; [e]Department of Geology & Geography, West Virginia University, Morgantown, WV, USA; [f]Institute of Earth Sciences, Uppsala University, Uppsala, Sweden; [g]Géosciences Environnement Toulouse (GET), Observatoire de Midi-Pyrénées, CNRS, IRD, Université Paul Sabatier, Toulouse, France; [h]Departamento de Geologia, Universidade Federal do Rio de Janeiro, Rio de Janeiro, Brazil; [i]Department of Earth Science, Paleobiology, Uppsala University, Uppsala, Sweden; [j]Department of Geology, Western Washington University, Bellingham, WA, USA; [k]Earth and Planetary Sciences, University of California Santa Cruz, Santa Cruz, CA, USA; [l]Centre for Geobiology, University of Bergen, Bergen, Norway; [m]Department of Urban Management, Kyoto University, Kyoto, Japan; [n]School of Geography, Earth Science and Environment, University of the South Pacific, Suva, Fiji; [o]Department of Organic Geochemistry, Institute of Geosciences, Christian-Albrechts-Universität zu Kiel, Kiel, Germany; [p]School of Physical Sciences and Centre of Excellence in Ore Deposits (CODES), University of Tasmania, Hobart, TAS, Australia; [q]Center for Advanced Marine Core Research, Kochi University, Nankoku, Japan; [r]Department of Earth and Atmospheric Sciences, University of Nebraska Lincoln, Lincoln, NE, USA; [s]College of Earth, Ocean and Atmospheric Sciences, Oregon State University, Corvallis, OR, USA; [t]Department of Earth Sciences, University of Bristol, Bristol, UK; [u]Instituto de Geología, Universidad Nacional Autónoma de México, Mexico, D.F., Mexico; [v]School of Geosciences, The University of Sydney, Sydney, NSW, Australia; [w]Department of Geological Sciences, University of Canterbury, Christchurch, New Zealand; [x]Department of Earth Science, Rice University, Houston, TX, USA; [y]GEOMAR Helmholtz Center for Ocean Research Kiel, Kiel, Germany; [z]Institute of Earth Sciences, Heidelberg University, Heidelberg, Germany; [aa]Geochemistry Division, Lamont-Doherty Earth Observatory of Columbia University, Palisades, NY, USA; [ab]Godwin Laboratory for Paleoclimate Research, Department of Earth Sciences, University of Cambridge, Cambridge, UK; [ac]Guangzhou Institute of Geochemistry, Chinese Academy of Sciences, Guangzhou, Guangdong, China

ABSTRACT

IODP Expedition 350 was the first to be drilled in the rear part of the Izu-Bonin, although several sites had been drilled in the arc axis to fore-arc region; the scientific objective was to understand the evolution of the Izu rear arc, by drilling a deep-water volcaniclastic section with a long temporal record (Site U1437). The Izu rear arc is dominated by a series of basaltic to dacitic seamount chains up to ~100-km long roughly perpendicular to the arc front. Dredge samples from these are geochemically distinct from arc front rocks, and drilling was undertaken to understand this arc asymmetry. Site U1437 lies in an ~20-km-wide basin between two rear arc seamount chains, ~90-km west of the arc front, and was drilled to 1804 m below the sea floor (mbsf) with excellent recovery. We expected to drill a volcaniclastic apron, but the section is much more mud-rich than expected (~60%), and the remaining fraction of the section is much finer-grained than predicted from its position within the Izu arc, composed half of ashes/tuffs, and half of lapilli tuffs of fine grain size (clasts <3 cm). Volcanic blocks (>6.4 cm) are only sparsely scattered through the lowermost 25% of the section, and only one igneous unit was encountered, a rhyolite peperite intrusion at ~1390 mbsf. The lowest biostratigaphic datum is at 867 mbsf (~6.5 Ma), the lowest palaeomagnetic datum is at ~1300 mbsf (~9 Ma), and the rhyolite peperite at ~1390 mbsf has yielded a U–Pb zircon concordia intercept age of (13.6 + 1.6/−1.7) Ma. Both arc front and rear arc sources contributed to the fine-grained (distal) tephras of the upper 1320 m, but the coarse-grained (proximal) volcaniclastics in the lowest 25% of the section are geochemically similar to the arc front, suggesting arc asymmetry is not recorded in rocks older than ~13 Ma.

CONTACT Cathy J. Busby ✉ cjbusby@ucdavis.edu 🖃 Department of Earth and Planetary Sciences, University of California Davis, One Shields Avenue, Davis, CA, 95616, USA

Introduction

This article provides an overview of shipboard results from one of three closely related International Ocean Discovery Program (IODP) expeditions carried out in sequence in the Izu-Bonin-Mariana (IBM) arc system in 2014 (Figure 1). It is meant to reach a wider audience than the scientific ocean drilling community, by presenting shipboard results in a compact and accessible manner, focusing on geologic results that will be of interest to those working in magmatic arcs on continents as well as those in the sea. More sophisticated geochemical results will be reported in future papers, using shore-based techniques; this article focuses on geologic observations, which will not change. We refer those seeking much greater detail to the *Proceedings of the International Ocean Discovery Program, Expedition 350*; all of the figures presented here appear in that volume, along with hundreds more (Tamura *et al.* 2015a, 2015d).

Expedition 350 was the first expedition to drill in the Izu rear arc; all previous IODP/ODP sites were drilled in or near the Izu-Bonin arc front or fore-arc (Figure 2), leading to an incomplete view of Izu arc magmatism. Thus, the main objective of Expedition 350 was to reveal the history of 'the missing half' of the subduction factory (Tamura *et al.* 2013). The second expedition (351) focused on IBM arc origins by drilling west of the Kyushu-Palau Ridge (Figure 1), where it was inferred that the foundation, origin, and early evolution of the IBM arc are recorded (Arculus *et al.* 2013, 2015). The third expedition (352) examined the processes of subduction initiation, by drilling the outer IBM fore-arc (Figure 1; Pearce *et al.* 2013; Reagan *et al.* 2015).

The goal of Expedition 350 was to core and log one site on the Izu rear arc, Site U1437 (Figure 1). This site was chosen to provide a temporal record of rear-arc magma compositions, ideally from Palaeogene to Neogene time, allowing comparison with the previously drilled fore-arc magmatic record and determination of across-arc geochemical variations throughout the history of the arc system. In addition to drilling in the rear arc, Expedition 350 also drilled a 150 m deep geotechnical hole in the fore-arc (Site U1436, Figure 1) for potential deep drilling; this site was chosen partly on the basis of results gotten from ODP Site 792, which is only 1.5 to the east of site U1436 (Tamura *et al.* 2015a). ODP Site 792 was drilled to 886 m below the sea floor (mbsf,) and the stratigraphy of its upper 150 m (Taylor and Fujioka *et al.* 1990) is very similar to that of Site U1436. Core from these sites yielded a rich record of late Pleistocene explosive volcanism (Tamura *et al.* 2015c), but is not discussed further here, for space

considerations. This article focuses on Site U1437, which was cored at 1776 m below sea level (mbsl) to
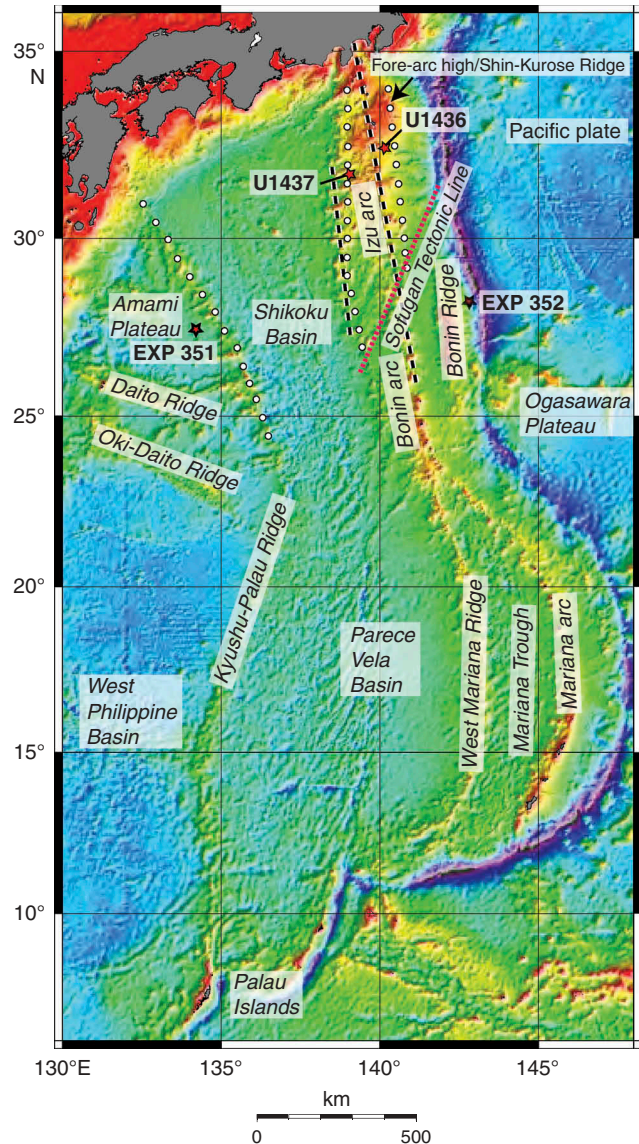

Figure 1. Tectonic setting of IBM arc (from Taylor 1992; Tamura and Tatsumi 2002). The IBM arc-trench system forms the convergent margin between the Pacific and Philippine Sea plates. Shown here are bathymetric features of the eastern Philippine Sea, IBM arc system, and Expedition 350 (Site U1436 in fore-arc and Site U1437 in rear arc) and Expedition 351 and 352 site locations (EXP). Dashed lines = wide-angle seismic profiles; the north–south seismic profiles (along the present-day arc front and rear arc ~150 km west of the arc front) are shown in Figure 4. Lines of circles = conspicuous north–south rows of long-wavelength magnetic anomalies, attributed to loci of Oligocene magmatic centres by Yamazaki and Yuasa (1998). Site U1436 is on the fore-arc anomaly (fore-arc high/Shin-Kurose Ridge); Site U1437 is on the rear-arc anomaly (Nishi-shichito Ridge). The boundary between the Izu arc and the Bonin arc lies at the Sofugan Tectonic Line, discussed further in Figure 4. Figure reprinted from Proceedings of the International Ocean Discovery Program, Expedition 350 (Tamura et al. 2015a) with permission from IODP.
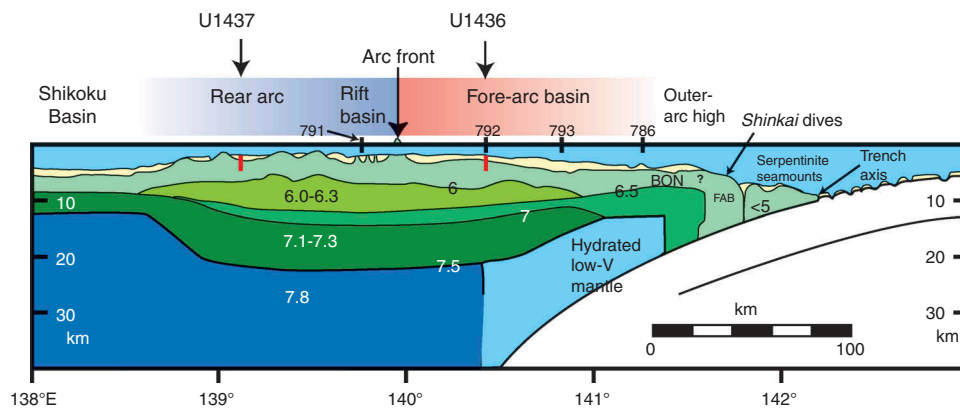
Figure 2. Wide-angle seismic profile across the Izu arc, with *P*-wave velocities for upper, middle, and lower crust (greens) and for mantle (blues) (Suyehiro *et al.* 1996). ODP (black) and IODP (red) sites are projected onto this line of section. Site U1437 is the first site drilled in the broad region of long-lived rear-arc seamount chains (shown in Figure 3). ODP Site 791 is also in the rear arc, but it is located in the narrow, young, and active Sumisu rift. Site U1436 and ODP Sites 792, 793, and 786 are in the modern fore-arc basin. BON = boninite, FAB = fore-arc basalt. Figure reprinted from Proceedings of the International Ocean Discovery Program, Expedition 350 (Tamura et al. 2015a) with permission from IODP.

a depth of 1806.5 mbsf, through a volcaniclastic succession, with excellent core recovery (Holes U1437 B, D, and E overall: 55%, 74%, and 62%). This provided a time-integrated view of the rear arc over the past ~14 million years.

Major questions addressed by drilling the Izu rear arc include the following: (1) Izu rear arc volcanoes differ from arc front volcanoes by being more similar to averaged continental crust (i.e. enriched in alkalis, Ba, Th, U, and LREE). The Izu rear arc is, therefore, important for understanding how arc magmas and intracrustal differentiation produce crust that is similar in composition to the 'averaged continental crust'. When did this arc asymmetry develop? (2) What kinds of basins accommodated the volcaniclastic succession we drilled? (3) What eruption, transport and depositional processes are recorded in the rear arc volcaniclastic succession targeted for drilling, and what kinds of depositional environments are represented by the succession?

Evolution of the IBM arc system

The IBM arc (Figure 1) has formed in response to subduction of the Pacific plate over the past 52 million year (Stern *et al.* 2003). Subduction began as part of a hemisphere-scale foundering of old, dense lithosphere in the western Pacific (Bloomer *et al.* 1995; Cosca *et al.* 1998). During the subduction initiation stage (~52–47 Ma) investigated by Expedition 352 (Figure 1), igneous activity successively produced low-K mid-ocean-ridge basalt (MORB)-like tholeiite, boninite, and subordinate low-K rhyolite across the region that now lies in the fore-arc (cf. Reagan *et al.* 2015). This suggests that sinking of the

downgoing plate was rapidly followed by an episode of asthenospheric upwelling and melting, sometimes enhanced by solute-bearing water fluxes released from the downgoing plate, over a zone that was thousands of kilometres long and as wide as 200 km (Reagan *et al.* 2010). As subduction proceeded, hydrous mantle melting overprinted decompression mantle melting, establishing the first mature arc in Eocene to Oligocene time, referred to as the Kyushu-Palau arc (Taylor 1992; Ishizuka *et al.* 2006a, 2006b, 2011), herein also referred to as the Palaeogene arc.

By ~25 Ma, rifting began along the length of the Kyushu-Palau arc and opening of the Shikoku Basin isolated the rear-arc volcanoes from the arc-front volcanoes (Ishizuka *et al.* 2011; Figure 1), producing the Kyushu-Palau Ridge remnant arc, which has Eocene and Oligocene rear-arc rocks (see Expedition 351 site, Figure 1). Seafloor spreading of the Shikoku and Parece Vela Basins (Figure 1) at ~25–17 Ma was likely accompanied by a hiatus in arc magmatism, but the fore-arc sedimentary record shows that arc-front volcanism resumed by ~17 Ma (Stern *et al.* 2003), referred to as the Neogene arc, or the IBM arc (Ishizuka *et al.* 2011).

The Neogene IBM arc front is inferred to lie in nearly the same position as the Palaeogene arc front (Ishizuka *et al.* 2011); however, pre-Quaternary rocks have not been recovered from the IBM arc front, perhaps because they are buried or were partly remelted and/or remobilized during the Quaternary. In contrast, the Izu rear arc (Figures 1 and 3) has not been extensively buried or modified by Quaternary magmatic processes, so Neogene rocks are well preserved; these are dominated by ~17–3 Ma NE-trending rear-arc seamount
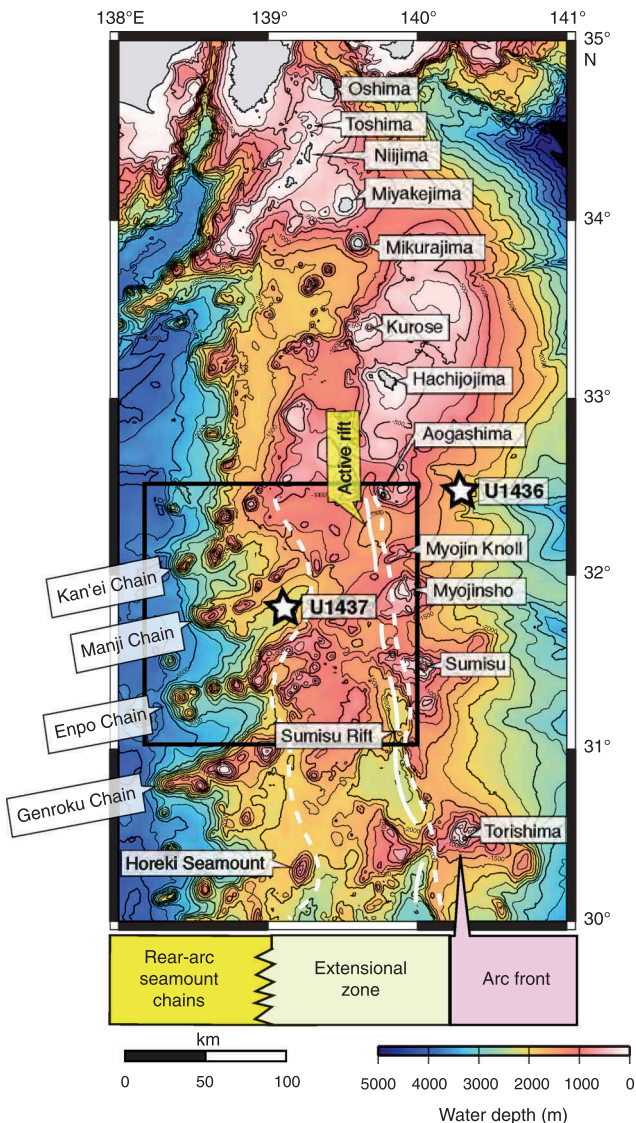
Figure 3. Volcano-tectonic domains within Izu arc. The well-defined arc front is formed by a ~north–south chain of island volcanoes, the largest of which are named here. Arc crust underlies the rear arc, whereas the Shikoku Basin (Figure 1), which forms the western boundary of the rear arc, is floored by oceanic crust. The rear arc is divided into two tectonic zones, from west to east (also oldest to youngest): (1) rear-arc seamount chains (~100-km long; ~17–3 Ma) which trend at a high angle to the arc front and span the compositional range from basalt to rhyolite, and (2) extensional zone (~100-km wide, <3 Ma), overlapping the eastern half of the rear-arc seamount chains, and characterized by ~north–south normal faults with small bimodal volcanoes (backarc knolls). Along the eastern margin of the extensional zone, immediately behind the arc front, lies a narrow active rift (<1 Ma), with north–south rift basins and bimodal volcanism. Volcanic rocks in the extensional zone and the active rift are referred to as rift-type magmas, and those in the rear-arc seamount chains are referred to as rear-arc seamount chain-type magmas. White stars = Site U1436 (fore-arc) and Site U1437 (rear arc). Box = area of Figure 7.

chains described in the following. The Marianas segment of the IBM arc (Figure 1) differs from the Izu segment by lacking the rear-arc seamount chains;

instead, a new episode of arc rifting began at ~7 Ma, resulting in opening of the Mariana Trough back-arc basin by seafloor spreading at ~3–4 Ma (Yamazaki and Stern 1997). Rifting of the Izu arc began at ~3 Ma behind the arc front (Figure 3).

We know more about the Neogene history of the IBM arc than we do about its Palaeogene history; yet it is thought that most of the IBM crust was generated in the Palaeogene (Eocene–Oligocene; Kodaira et al. 2008). Furthermore, silicic volcanoes of the Quaternary arc front and Miocene granitic rocks in the Izu collision zone on Honshu are inferred to have formed by melting of Eocene–Oligocene arc crust (Tamura et al. 2009, 2010). As discussed in the following, Neogene rhyolite volcanism may be more important in the Izu rear-arc seamount chain than previously thought and could have resulted from melting of Palaeogene 'arc basement'. For this reason, we will now review the evidence for Palaeogene arc basement highs in the Izu arc and discuss constraints on their age and origin.

Palaeogene arc basement highs in the Izu arc

Magnetic and seismic surveys indicate that both IODP Sites U1436 and U1437 lie along buried north–south ridges that consist of magmatic crystalline rocks, which are inferred to be Oligocene–Eocene (Palaeogene) in age. Three conspicuous, approximately north–south rows of long-wavelength magnetic anomalies were identified by Yamazaki and Yuasa (1998) in the Izu-Bonin arc system and attributed to loci of middle- to lower-crustal magmatic bodies (Figure 1):

- The western north–south anomaly corresponds to the Kyushu-Palau Ridge, where Eocene and Oligocene lava was dredged; these have rear-arc geochemical affinity, and are interpreted as rear-arc magmas rifted off the Palaeogene arc during the opening of the Shikoku Basin (Kodaira et al. 2008; Ishizuka et al. 2011).
- The eastern north–south anomaly lies in the modern fore-arc near the arc front and corresponds to the Shin-Kurose Ridge (Figure 1) (Yamazaki and Yuasa 1998), also referred to as the Izu fore-arc high (Taylor and Fujioka et al. 1990). The Shin-Kurose Ridge/fore-arc high forms a bathymetric high in the northern Izu arc and is buried beneath Oligocene to Quaternary volcaniclastic and sedimentary rocks in the southern Izu arc, at Ocean Drilling Program (ODP) Site 792 and Site U1436. Andesite lava in the lowermost 82 m at Site 792 was referred to as 'Oligocene basement', on the basis of K/Ar ages (Taylor and Fujioka et al. 1990;
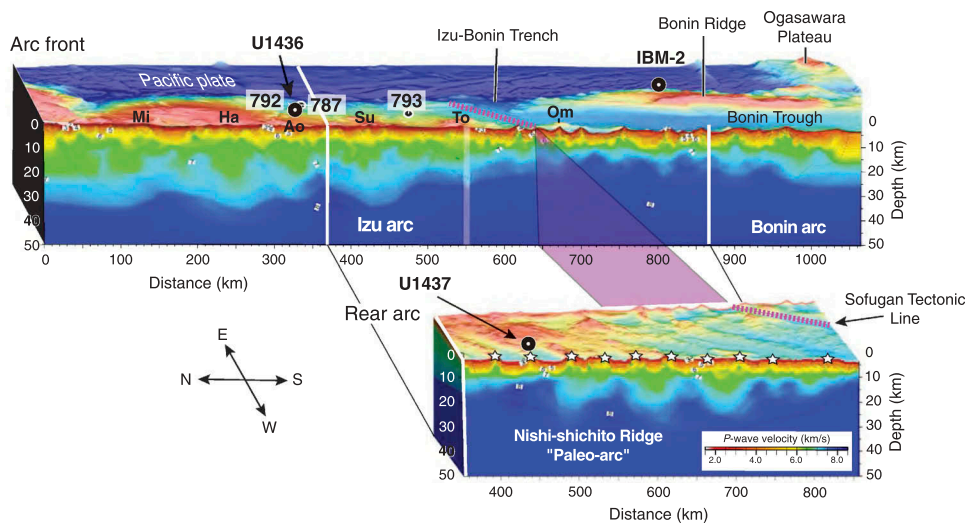
Figure 4. Wide-angle seismic profiles (Kodaira *et al.* 2008) showing middle-crust thickness variations in two transects: one along the arc front and one along the rear-arc Nishi-shichito Ridge; the positions of these lines are shown as lines of circles on Figure 1. The 6.0–6.8, 7.1–7.3, and 7.8 km/s layers (see P wave velocity on key) correspond to middle crust, lower crust, and upper mantle, respectively. Based on variations in middle-crust thickness in these profiles, Kodaira *et al.* (2008) infer that rear-arc crust was obliquely rifted off the arc front, probably during the opening of the Shikoku and Parece Vela Basins (~25 Ma; Figure 1). Quaternary basalt-dominant island volcanoes on the arc front: Mi = Miyakejima, Ha = Hachijojima, Ao = Aogashima, Su = Sumisu Caldera, To = Torishima; andesite Oligocene volcano east of arc front: Om = Omachi Seamount. ODP Sites 787, 792, and 793 also shown. Figure reprinted from Proceedings of the International Ocean Discovery Program, Expedition 350 (Tamura et al. 2015a) with permission from IODP.

Taylor 1992), but more recent ^{40}Ar/^{39}Ar dating show these are Eocene (Ishizuka *et al.* 2011).

- The central north–south magnetic anomaly lies buried in the Izu rear arc (Figure 1) and is referred to as the Nishi-shichito Ridge (Figure 4) (Yamazaki and Yuasa 1998). This basement high has not been drilled and was one of the objectives of Expedition 350. Kodaira *et al.* (2008) ran a wide-angle seismic profile along the length of the rear-arc Nishi-shi-chito Ridge and compared it to a wide-angle seismic profile made along the length of the arc front by Kodaira *et al.* (2007a, 2007b) (Figure 4). They divided the arc front into segments based on variations in the thickness of middle crust and did the same for the rear-arc Nishi-shichito Ridge. They concluded that although the thickness of the middle crust for each rear-arc segment is smaller than the thickness in the arc front, the bulk compositions of the crust segments are inferred to be the same, on the basis of seismic properties.. Furthermore, they used the match on middle crustal thicknesses to infer that the Nishi-shichito Ridge is a 'palaeo-arc' that obliquely rifted off the arc front in an extension direction parallel to the northeast–southwest Sofugan Tectonic Line (Figure 1). The Sofugan Tectonic Line is the boundary between the Izu and Bonin arc segments (Figure 1); south of it lies the prominent
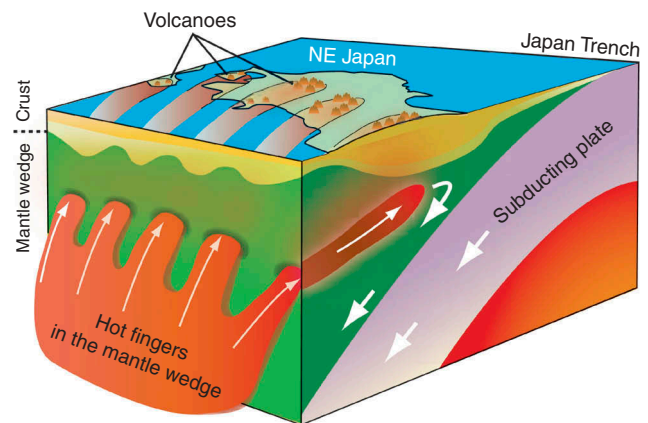

Figure 5. Hot fingers hypothesis of Tamura *et al.* (2002) proposed for northeast Japan and adapted here for the origin of Izu rear-arc seamount chains. Hypothetically, mantle convection above the subducting slab produces finger-like hot regions in the mantle wedge below the rear-arc plate. These hot regions extend towards the arc front with time, suggesting younging of rear-arc seamounts from west to east. Figure reprinted from Proceedings of the International Ocean Discovery Program, Expedition 350 (Tamura et al. 2015a) with permission from IODP.

Bonin Ridge and the deep fault-bounded Ogasawara Trough to the west, produced by Eocene to early Oligocene arc magmatism and back-arc extension, respectively. Both the prominent arc ridge and the fault-controlled back-arc basin are absent north of the Sofugan Tectonic

Line, so we infer that the Sofugan Tectonic Line originated as an accommodation fault between a region of high extension to the south and little or no extension to the north. Kodaira *et al.* (2008) propose that oblique rifting of the Nishi-shichito Ridge palaeoarc off the arc front occurred during the opening of the Shikoku Basin, sometime after ~30 Ma. If the oblique rifting model is correct, the crystalline basement beneath Site U1437, not reached during Expedition 350, may represent rear-arc crust but formed in a position much closer to the arc front than it is now; alternatively, it may represent arc-front crust that has become stranded in the rear arc by rifting. New seismic surveys undertaken in preparation for drilling at Site U1437, described in the following, also support the interpretation that the rear arc is underlain by Palaeogene arc basement rocks.

Neogene rear-arc volcanism, Izu arc

We refer to all Neogene volcanic rocks behind the Izu arc front as rear-arc volcanic rocks. Rear-arc volcanic rocks (Figure 3) include (1) the ~17–3 Ma east NE-trending basaltic to rhyolitic rear-arc seamount chains, (2) the <3 Ma bimodal back-arc knolls of the broad extensional zone, and (3) the <1.5 Ma bimodal volcanic rocks of the active rift immediately behind the arc front. Thus, Izu rear-arc volcanism falls into two magmatic suites: the <3 Ma bimodal rift-type magmas and the ~17–3 Ma basalt to rhyolite rear-arc seamount-type magmas. Both types lie within the rear part of the arc (i.e. behind the arc front) and lie on arc crust, although the westernmost end of the rear-arc seamount chains lies on Shikoku Basin oceanic crust. The bimodal rift-type magmas differ from both the arc front and the rear-arc seamount chains in trace element and radiogenic isotopic ratios; this has been variably attributed to (1) a transition from flux to decompression mantle melting as arc rifting commences, (2) a change in the character of slab-derived flux, or (3) a change in the mantle source through mantle wedge convection (Hochstaedter *et al.* 1990a, 1990b, 2001; Ishizuka *et al.* 2003a, 2006b; Tollstrup *et al.* 2010).

The Izu rear-arc seamount chains are as long as ~80 km and strike N60°E (Figure 3). The tops of the Izu rear-arc volcanic chains were sampled by dredging, and their compositions range from basalt to rhyolite (Ishizuka *et al.* 1998, 2003b; Hochstaedter *et al.* 2000). Three main hypotheses have been proposed for the origin of the seamount chains:

(1) They are related to compression caused by collision between the southwest Japan and Izu arcs, associated with opening of the Japan Sea (Karig and Moore 1975a; Bandy and Hilde 1983).
(2) They formed along Shikoku Basin transform faults (Yamazaki and Yuasa 1998).
(3) They overlie diapirs in the mantle wedge, such as the 'hot fingers' proposed for northeast Japan (Tamura *et al.* 2002), illustrated in Figure 5.

A striking characteristic of volcanic arcs is the asymmetry in geochemical characteristics with distance from the trench, which was known prior to the advent of plate tectonics (Kuno 1959; Dickinson and Hatherton 1967). Izu arc-front rocks are low-K, but the rear-arc type lava is medium to high-K (Gill 1981). Similarly, arc-front volcanic rocks are strongly depleted in incompatible light rare earth elements (REEs) relative to the middle and heavy REEs, whereas lava from rear-arc seamount chains is enriched in light REEs. On both K_2O *versus* SiO_2 and REE plots, the composition of the rear-arc seamount chain magmas is more similar to the continental crust composition than the arc-front magmas. Thus, the Izu rear-arc magmatism and crust formation appears to be a better analogue to generate continental crust than the arc front (Tamura *et al.* 2013).

Site U1437 lies in an ~20-km wide basin in the low area between two major constructional volcanic ridges: the Manji and Enpo rear-arc seamount chains (Figure 3). It is therefore classified as a volcano-bounded intra-arc basin, using the criteria elucidated by Smith and Landis (1995) (Figure 6). In contrast, the active rift to the east of Site U1437 (Figure 3) is a fault-bounded intra-arc basin, using the terminology of Smith and Landis (1995) (Figure 6). For simplicity, the volcano-bounded basin bounded by the Enpo and Manji rear-arc seamount chains (Figure 7) is referred to as the Enpo-Manji volcano-bounded basin (Figure 8(c,d)). Similarly, we propose that future workers refer to other basins between rear-arc seamount chains by the names of the chains that bound them (e.g. Genroku-Enpo Basin and Manji-Kan'ei Basin, Figure 3).

New descriptive scheme for volcaniclastic rocks

Expedition 350 devised a new scheme for describing volcaniclastic and associated nonvolcaniclastic sediments, described in detail by Tamura *et al.* (2015b). The new scheme was devised to improve description of volcaniclastic sediments and their mixtures with nonvolcanic (siliciclastic, chemical, and biogenic) sediments but maintain the usefulness of prior schemes for describing nonvolcanic sediments. The new scheme

was devised to facilitate the understanding of volcano-sedimentary processes by making reproducible and quantifiable observations of volcanic input to the sedimentary record. Previous core descriptions (e.g. ODP Leg 126) obscured the importance of volcanic input by referring to volcanic material (e.g. ashes/tuffs) as siliclastic material (e.g. sands/sandstone or tuffaceous sands/sandstones). The new classification scheme is based entirely on observations that can be made by any scientist at the macroscopic and microscopic level, making the data more reproducible from user to user. Genetic inferences are not part of the descriptive scheme but can be added as comments to descriptive records if so desired. A very brief description of the scheme is presented here to allow the reader to understand our rock descriptions.

Four sedimentary lithologic classes were defined, including: (1) volcanic lithologic class, defined as >75% volcanic particles; (2) tuffaceous lithologic class, containing 25–75% volcanic-derived particles mixed with non-volcanic particles; (3) nonvolcanic siliciclastic lithologic class, containing <25% volcanic siliciclastic particles, where nonvolcanic siliciclastic particles dominate chemical and biogenic particles; (4) biogenic lithologic class, containing <25% volcanic and nonvolcaniclastic siliciclastic and chemical particles. The principal name for sediments and sedimentary rocks is based on grain size and is purely descriptive; it does not depend on interpretations of fragmentation, transport, or depositional or alteration processes. The sedimentary grain size classes of Wentworth (1922) are used for the nonvolcanic siliciclastic and tuffaceous lithologic classes, whereas the grain size classes of Fisher and Schmincke (1984) are used for the volcanic lithologic class. The prefix 'monomict' was applied where clast compositions were restricted to a single type and 'polymict' was applied where clast compositions of multiple types were present. We adopted a new method to estimate the compositional range of volcanic clasts using three entries: 'mafic', 'evolved' and a mixture of the two, termed 'bimodal'. In our macroscopic analyses, mafic *versus* evolved intervals were defined by the greyscale index of the main particle component, with mafic grains and clasts usually ranging from black to dark grey and evolved grains and clasts ranging from dark grey to white. Microscopic examination further aided in assigning the prefix 'mafic' or 'evolved', using glass shard colour and mineralogy. Intervals we described as mafic are inferred to be basalt and basaltic andesite, and intervals we described as evolved were inferred to be intermediate and silicic in composition; however, precise determination of bulk composition requires chemical analysis.
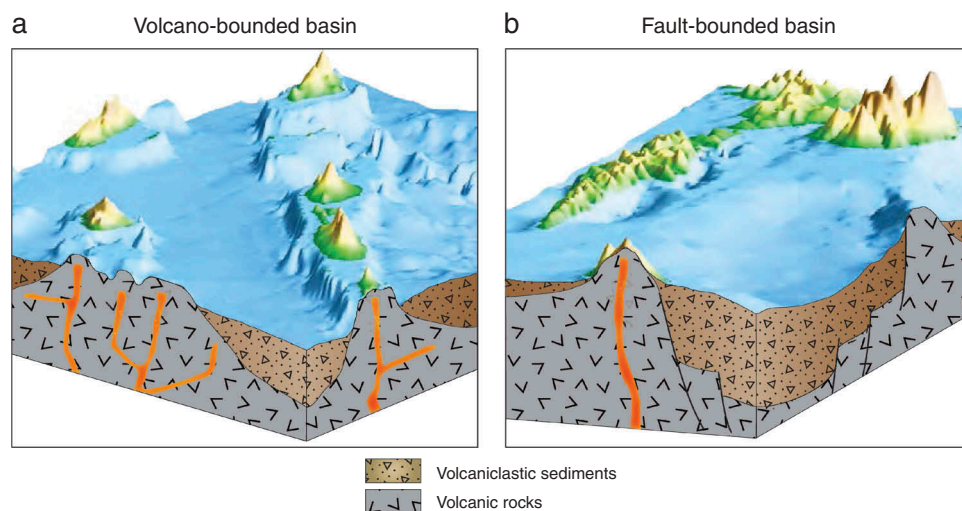

Figure 6. Two main basin types recognized within arcs, as defined by Smith and Landis (1995). (a) Volcano-bounded basin: small, irregular basins between individual volcanoes; larger linear troughs between volcanic chains; and thick basin fill preserved only in oceanic arcs, below sea level. Low areas between the series of rear-arc seamount chains shown in Figure 3 are volcano-bounded basins formed during growth of the chains between ~17 and 3 Ma. Site U1437 is located in one of these volcano-bounded basins, which we refer to as the Enpo-Manji Basin (Figures 7 and 8(c,d)). (b) Fault-bounded basin: rapidly subsiding basins that are deep (up to 10 km) and have very high sediment accumulation rates (~1 km/million year); they are found in continental and oceanic arcs. A fault-bounded basin is currently forming in the <1 Ma active rift west of the Izu arc front (Figure 3). Although the broader zone of extension (<3 Ma) produced faults within the eastern halves of the volcano-bounded basins between the rear-arc seamount chains, including the basin drilled at Site U1437 (some visible on Figure 8(c,d)), the bounding volcanic chains (and not the <3 Ma extensional zone faults) primarily controlled accommodation (Figure 8(c)). Figure reprinted from Proceedings of the International Ocean Discovery Program, Expedition 350 (Tamura et al. 2015a) with permission from IODP.

Figure 7. Bathymetric maps of rear-arc region behind the arc-front volcanoes (location on Figure 3). (a) Unannotated and annotated bathymetric maps, showing named volcanoes and $^{40}Ar/^{39}Ar$ and K–Ar ages in Ma from Ishizuka et al. (2003b). Age groups: ~12.5–3 Ma rear-arc basalt to rhyolite seamount volcanoes, <3 Ma bimodal volcanic rocks in extension zone that overlaps eastern half of the rear-arc seamount chains, and <1 Ma bimodal volcanic rocks of the narrow active rift (Figure 3). Site U1437 lies in a volcano-bounded basin (Figure 6(a)) between the Manji and Enpo rear-arc seamount chains at the foot of flat-topped Manji Volcano, presumably planed by wave action. (b) Positions of JAMSTEC surveys (Yamashita et al. 2015) shown in Figure 8. Figure reprinted from Proceedings of the International Ocean Discovery Program, Expedition 350 (Tamura et al. 2015a) with permission from IODP.

In summary, the new volcaniclastic descriptive scheme applied during Expedition 350 uses a more nongenetic approach than proposed by previous authors because the sediments and rocks are named based on materials that are visible macroscopically and microscopically and not on the basis of inferred fragmentation, transport, and depositional processes (i.e. pyroclasts, autoclasts, hydroclasts, epiclasts, and reworked volcanic clasts [Fisher and Schmincke 1984; Cas and Wright 1987; McPhie et al. 1993).

International Ocean Discovery Program Site U1437

Site U1437 is located in the Izu rear arc and is ~330 km west of the axis of the Izu-Bonin Trench (Figures 1 and 2) and ~90 km west of the arc-front volcanoes Myojinsho and Myojin Knoll (Figure 3) at 2117 mbsl between the Manji and Enpo seamount chains (Figure 7). The stratigraphic section shown in Figure 9 is a composite from three holes drilled a few tens of metres apart using different techniques. The shallowest and least consolidated material was penetrated at Hole U1437B (drilled using Advanced Piston Coring (APC), Half-Length Advanced Piston Corer (HLAPC), and Extended Core Barrel (XCB)). Deeper, more consolidated units were drilled at Holes U1437D and U1437E using the Rotary Core Barrel (RCB) (see http://iodp.tamu.edu/tools/for details about these tools). These different drilling techniques resulted in partial sampling of the section: In Hole U1437B we cored 439.1 m and recovered 242.6 m (55% recovery). In Hole U1437D we cored 677.4 m, with 503.8 m recovered (74%). In Hole U1437E we cored 702.5 m and recovered 387.45 m (55% recovery). Incomplete and disturbed cores are unfortunate but expected; to ensure a more uniform perspective on the section (including intervals that are not recovered in cores), downhole logging is carried out before the hole is cased. Combined studies of cores and well logs allowed the entire sequence to be interrogated. Most of the unconsolidated stratigraphy in Hole U1347B is well preserved and few coring disturbances occur, allowing very good stratigraphic continuity. Drilling disturbances are present in Holes U1347D and U1347E, and vary depending on rock type and consolidation.

Seismic surveys

Seismic surveys for Site U1437 are summarized briefly here. Numerous lines were shot in two different campaigns (Yamashita et al. 2017); parts of three seismic sections that cross at Site U1437 are plotted on Figure 7 (c) and shown in Figure 8. Line IBr5 (Figure 8(a)) is the longest seismic line, running east–west from the Manji
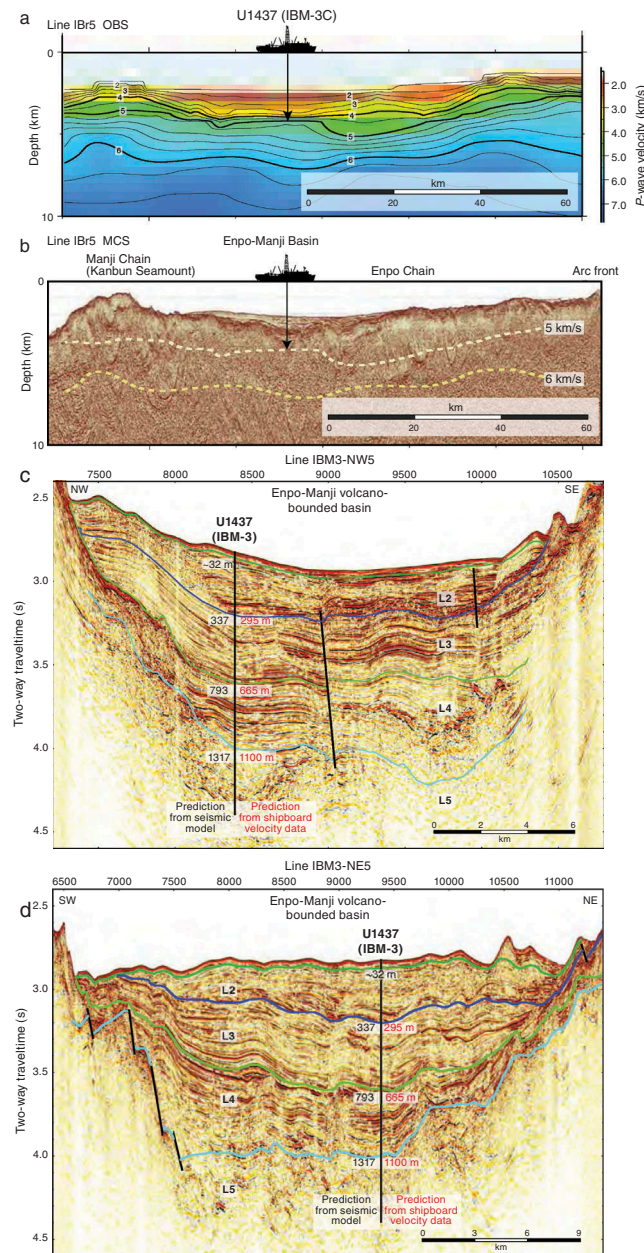
Figure 8. Three seismic lines, crossing at Site U1437; positions plotted on Figure 7(b). Line IBr5 is the longest, an ~E–W line that runs from the Manji rear-arc seamount chain in the west to the arc front in the east. This is shown as: (a) line IBr5 OBS: seismic velocity image obtained from wide-angle OBS data, with OBSs deployed every 5 km along line IBr5, and (b) line IBr5 MCS, depth-converted MCS reflection profile; dashed yellow lines = iso-velocity contours of 5 and 6 km/s obtained from seismic velocity image in (a), which are interpreted as the depth to igneous basement (upper crust) and middle crust, respectively. Seismic lines with interpreted seismic layers are shown in (c) and (d), running transverse to the Enpo-Manji volcano-bounded basin (c) and along the axis of the basin (d). On (c), the Manji volcano lies on the northwest, with $^{40}Ar/^{39}Ar$ ages of 6.86 and 6.53 Ma, and an unnamed volcano lies on the southeast, with an $^{40}Ar/^{39}Ar$ age of 1.96 Ma (see Figure 7). On (d), an unnamed volcano lies on the southwest, with a 40Ar/39Ar age of 12.35 Ma; minor north–northwest faults lie transverse to the volcano-bounded basin, parallel to normal faults in the broad extensional zone to the east (Figure 3). The north–northwest faults appear to have been active prior to the deposition of Layer L3 but do not provide the primary accommodation.

rear-arc seamount chain across the Enpo seamount chain to the arc front; it was shot both by wide-angle ocean-bottom seismometer (OBS, Figure 8(a)) and by multichannel seismic (MCS, Figure 8(b)). The wide-angle OBS survey shows the velocity structure of the upper

~10 km, and the MCS line shows the upper ~5 km. Generally, the velocity transition to >5 km/s is thought to represent the transition to igneous rocks, perhaps representing arc upper crust lava or crystalline rocks, and the velocity transition to 6 km/s is generally
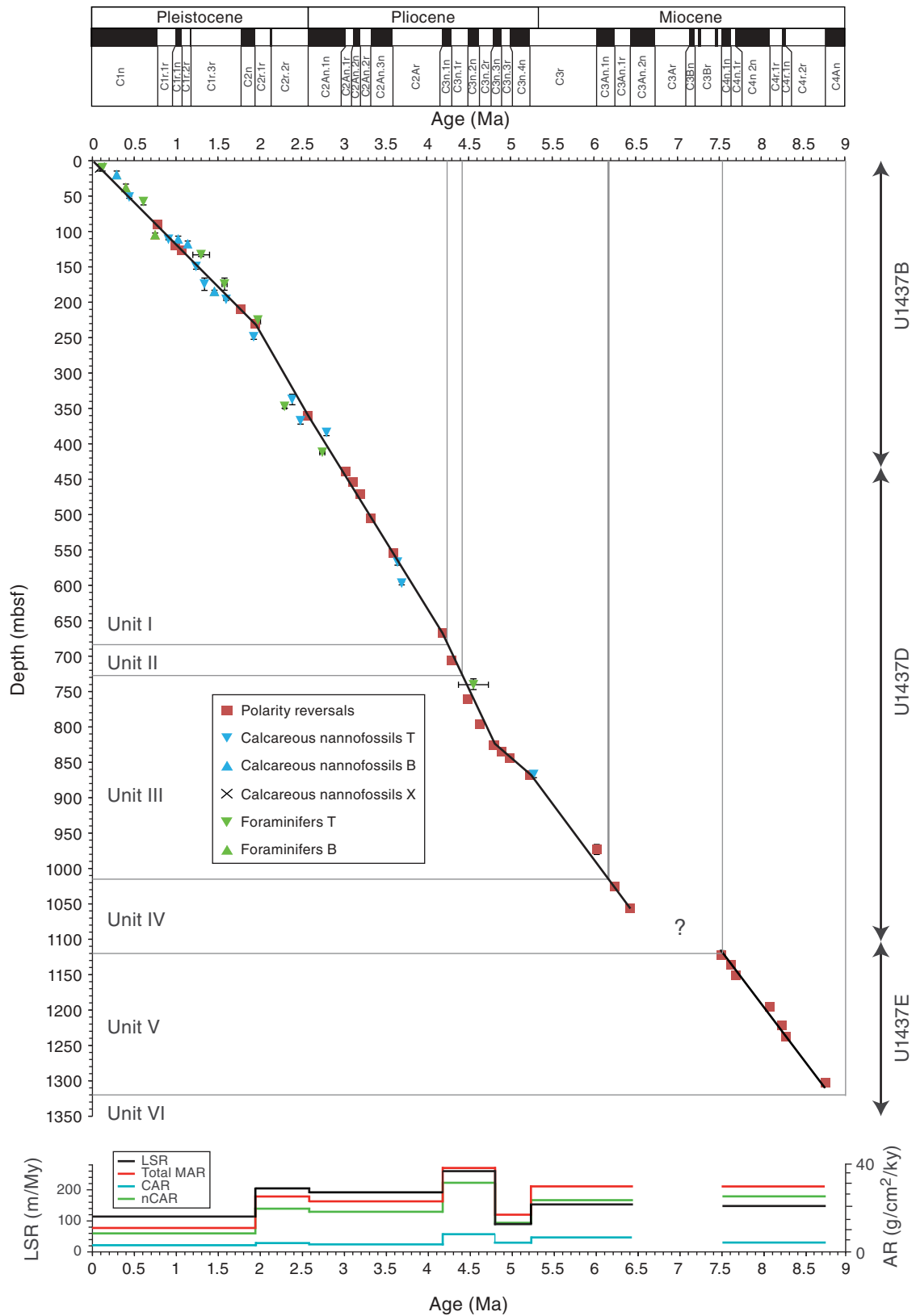
Figure 9. Age-depth model for Site U1437. Shown are shipboard biostratigraphic and magnetostratigraphic datums, and linear sedimentation rates (LSR)/mass accumulation rates (MAR). MARs are calculated using LSR derived from the age-depth model and dry bulk density calculated from shipboard moisture and density (MAD) analyses. MARs of carbonate (CAR) and noncarbonated (nCAR) are calculated by multiplying the MAR by carbonate weight per cent, calculated from shipboard coulometry measurements of inorganic carbon weight per cent. T = top, B = bottom, X = crossover.
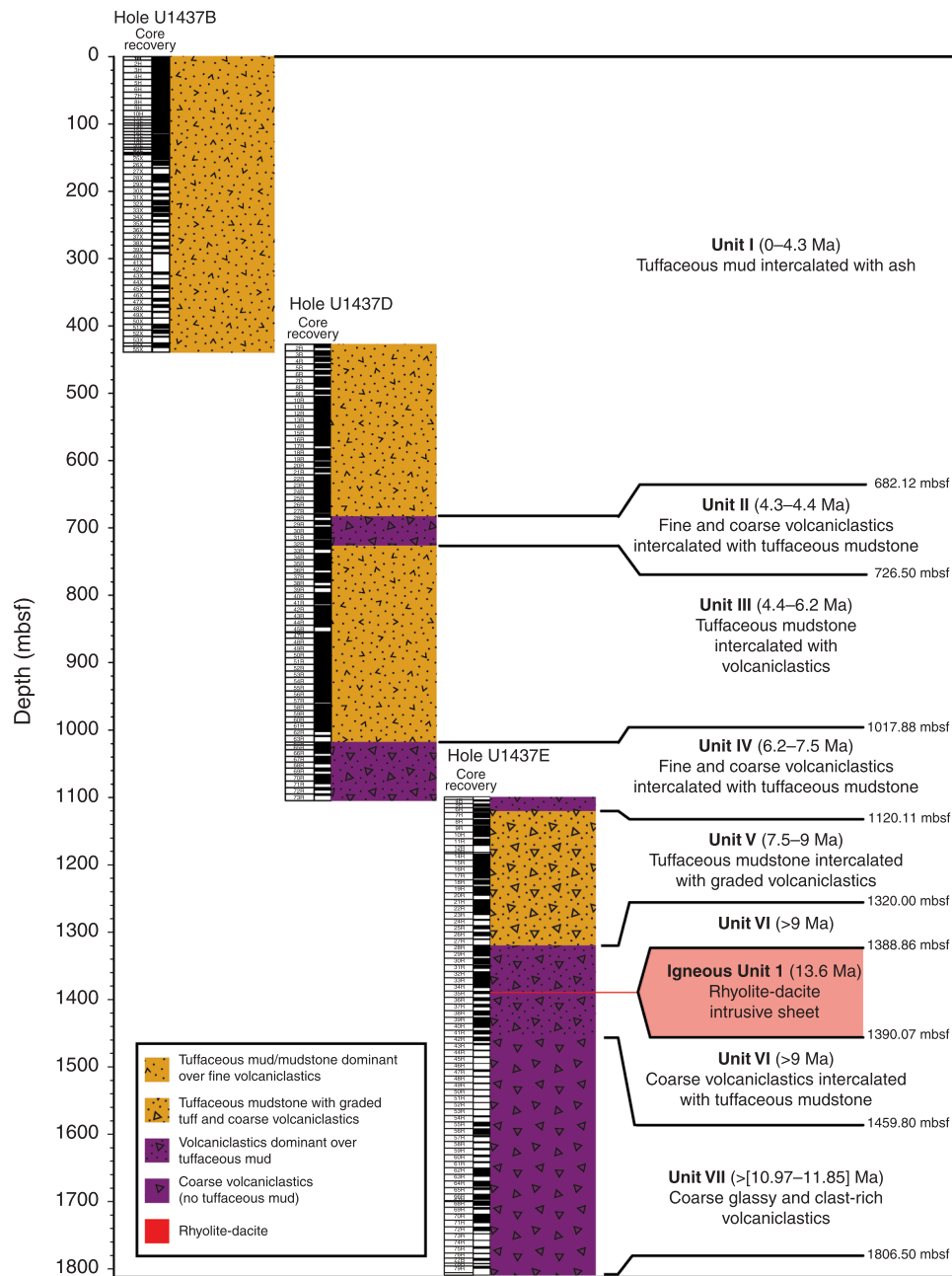
Figure 10. Summary lithostratigraphic log for Site U1437. The boundary between coarse- and fine-grained volcaniclastics is 2 mm (corresponding to the boundary between ash and lapilli-sized particles). Representative core photos for Lithostratigraphic units I through VI and Igneous unit I are shown in Figures 11–18.

thought to represent the transition to middle crust (see boundaries picked in Figure 8(b)). Tamura *et al.* (2013) estimated the 5 km/s iso-velocity contour to lie at ~2100 mbsf at Site U1437 and suggested that these rocks could be Oligocene–Eocene 'igneous basement', consisting of lava and/or intrusions. Line IBM3-NW5 (Figure 8(c)) clearly shows that Site U1437 lies in a volcano-bounded basin between the Enpo and Manji rear-arc seamount chains.

Age model

Site U1437 was drilled to a depth of 1804 mbsf in three holes (U1437B, U1437D, and U1437E), which we divide into seven lithostratigraphic units and one igneous unit (Figures 9 and 10). The biochronology for Site U1437 was established based on planktonic foraminifers and calcareous nannofossils (Figure 9). Both fossil groups show that the upper 1403 m of the succession spans
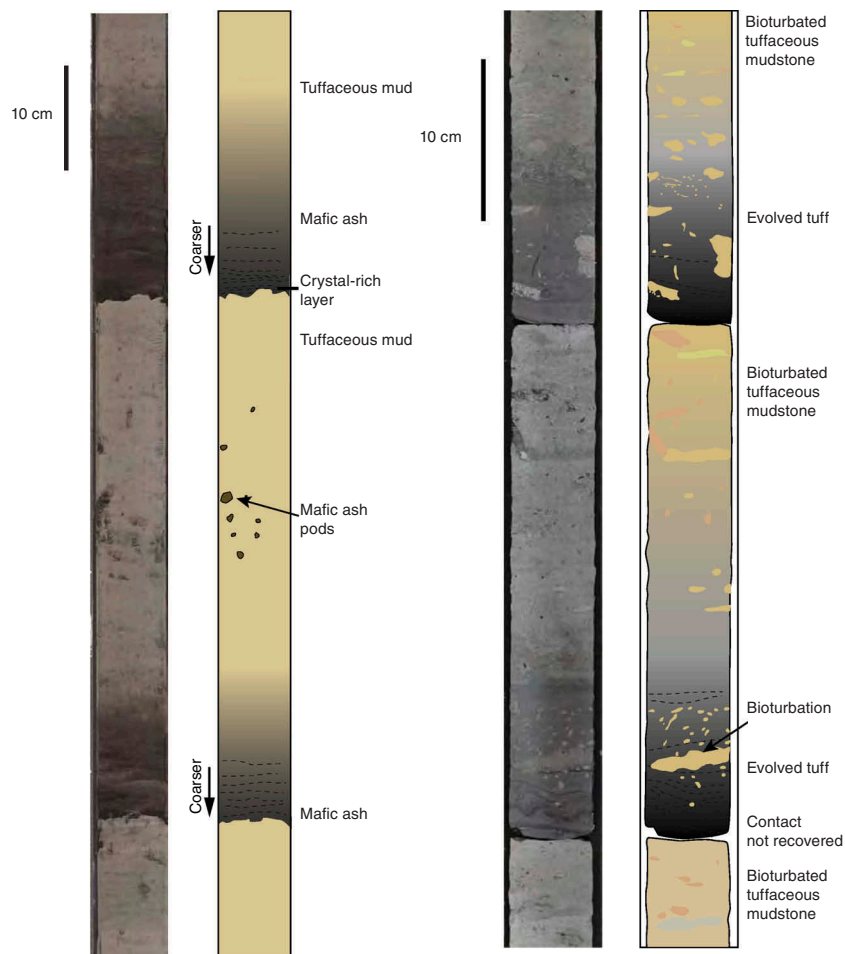
Figure 11. Unit I, representative core photos and interpretations: (Left pair) 5–10 cm mafic ash intervals with sharp bases and tops grading upward into tuffaceous mud, with mafic ash pods. (Right pair) Evolved tuff intervals grading upward into tuffaceous mud and bioturbation.

from the lower Pleistocene to the upper Miocene (maximum age detectable was ~11–12 Ma), and the timing of bioevents agrees well with magnetostratigraphic data. Deeper than 1403 mbsf, bioevents were difficult to establish because of poor preservation and low microfossil abundance (Figure 9), corresponding to a lithologic change from a succession dominated by tuffaceous mud/mudstone to one dominated by volcanic material (Figure 10).

We infer that a normal fault at the base of Hole U1437D was responsible for drilling problems there, including low recovery and more fractured rock. This forced us to drill a new hole (Hole U1437E) which started at the same sub-bottom depth as the base of Hole U1437D.; the first core was also fractured but cores below that were not. The fault is not obvious in the seismic section (Figure 8(c,b)) but it is not excluded either. On the basis of palaeomagnetic results (Tamura *et al*. 2015a), this normal fault is inferred to have caused a loss of section between the two holes (Figure 9). Magnetostratigraphy could

then be followed down as far as the top of Chron C4An (8.771 Ma) at 1302 mbsf (unit V, Figure 9). The age model does not extend into units VI and VII (Figure 9) because magnetostratigraphy was impossible to recognize, with the exception of reversed polarity seen at 1389.35 mbsf in igneous unit I, which indicated that coring had proceeded below the base of normal Chron C5n.2n (9.984–11.056 Ma; Tamura *et al*. 2015a) spanning the upper part of the lowest nannofossil age range. One additional age control point was added immediately postcruise: Igneous unit I is a rhyolite intrusive sheet with peperite margins (at 1389–1390 mbsf, Figure 10), described further later, which indicate that it is penecontemporaneous with the volcaniclastic section that encloses it (unit VI, Figure 10). In-situ measurement of zircons within magnetite crystals in the rhyolite intrusion yielded a preliminary U–Pb age of 13.6 Ma ±1.7 (n = 9) (Schmitt, pers. comm., 2014; Andrews *et al*. 2015; Konrad *et al*. 2016). Thus, we tentatively infer that the age of units VI and VII is ca. 9–14 Ma.
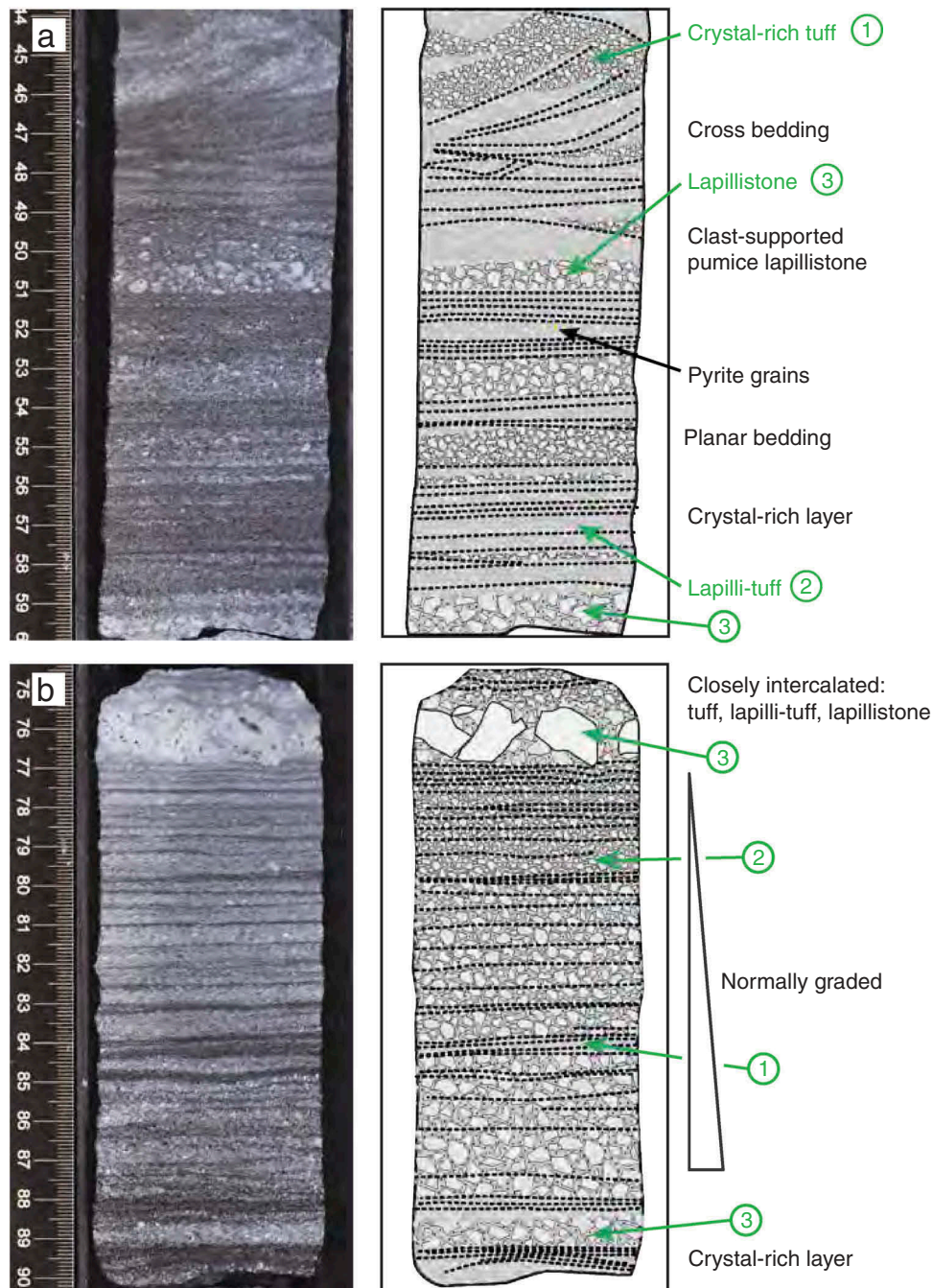
Figure 12. Unit II, core photos and line drawings of closely intercalated monomictic tuff, lapilli-tuff, and lapillistone, showing stratification, cross stratification, and normal grading. Crystal-rich tuff (1), lapilli-tuff (2), and lapillistone (3) in planar and cross-bedded intervals.

Description and interpretation of lithostratigraphic units

Lithostratigraphic units I–VII (Figure 10) are distinguished from each other based on the proportion and characteristics of tuffaceous mud/mudstone and interbedded tuff, lapilli-tuff, and tuff-breccia. Visual description of core was supplemented by 13 smear slides from Hole U1437B, and thin sections from Holes U1437B, U1437D, U1437E (5, 63, and 93, respectively). Mineralogy was done by macroscopic

and microscopic description; the shipboard XRD unit was not working so more detailed clay mineralogy was not done. The tuffaceous mud/mudstone is strongly to intensely bioturbated. Alteration becomes more pervasive and increases in intensity downhole; it is initially predominantly glauconitic–smectitic and eventually becomes more chloritic. The transition from unconsolidated to lithified rocks occurred progressively; however, the change to RCB drilling provides a useful approximation of the transition
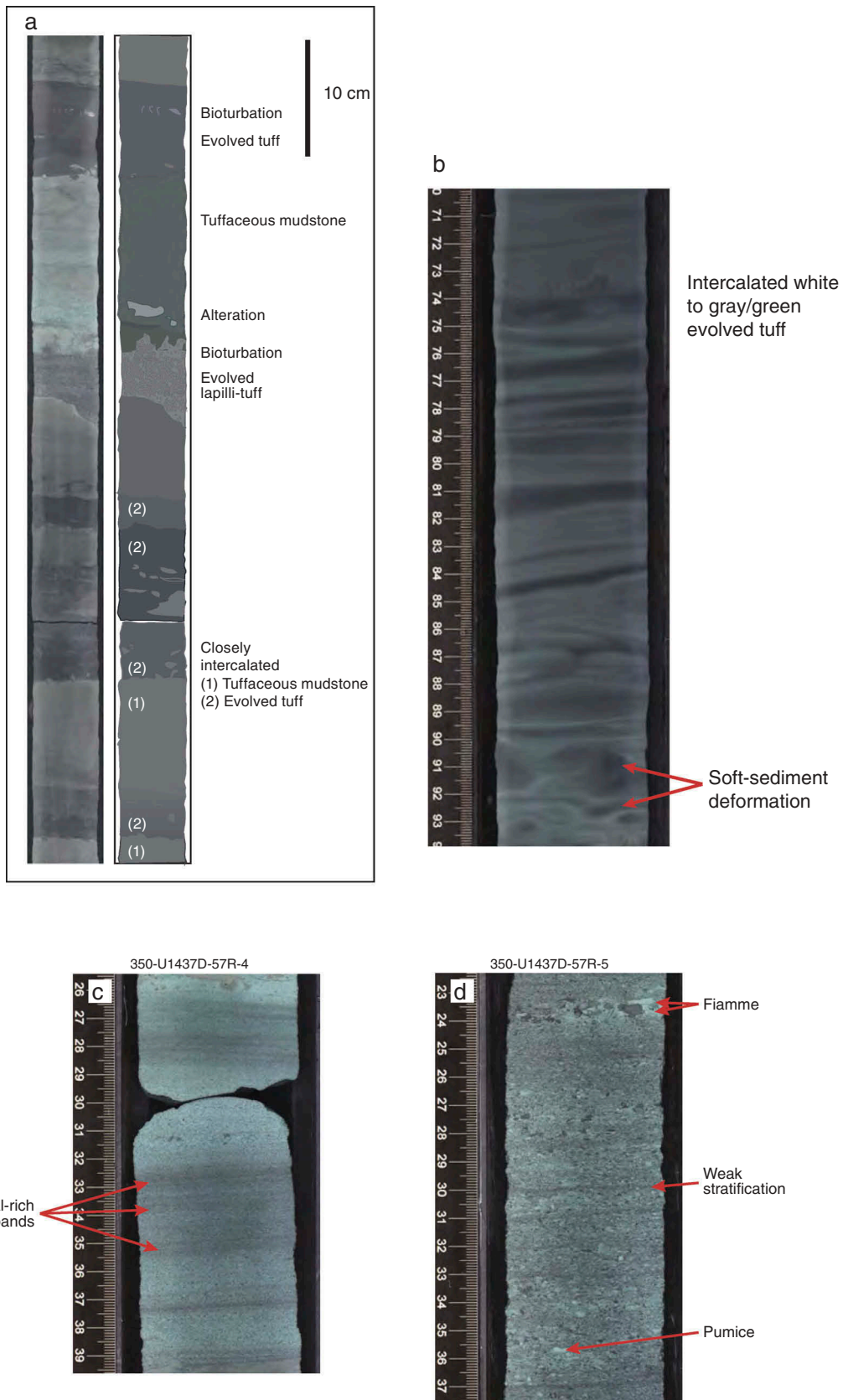
Figure 13. Unit III, core photos: (a) Alternating intervals of tuffaceous mudstone, evolved tuff, and evolved lapilli-tuff. (b) Intercalated white to grey-green evolved tuff, including soft-sediment deformation. (c) Crystal-rich stratified interval. (d) Fiamme-rich (with flattened pumice) and (nonflattened) pumice-rich intercalated layers.
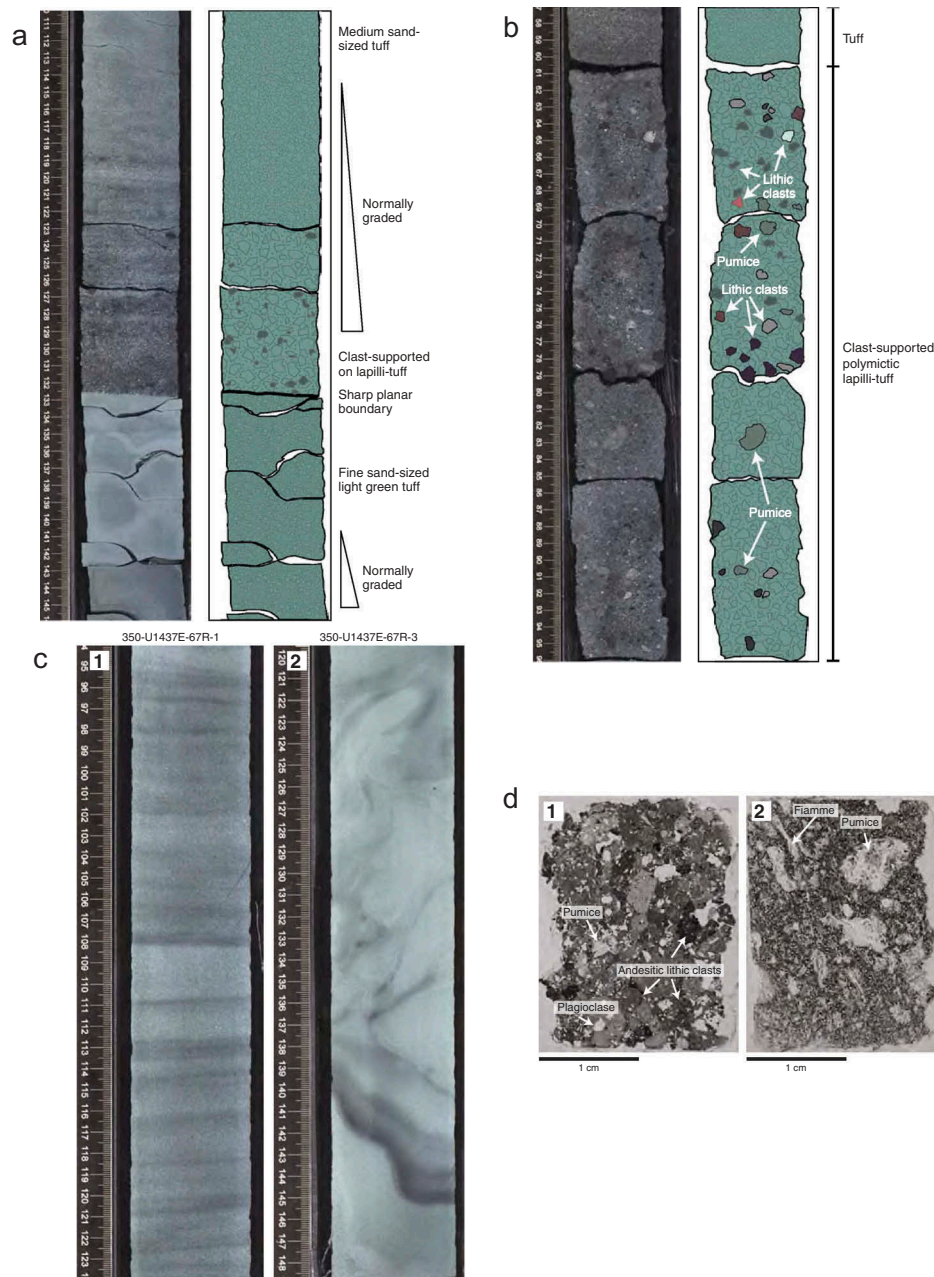
Figure 14. Unit IV: (a) Line scan and schematic drawing showing tuff, clast-supported polymictic lapilli-tuff, and fine-grained light green tuff lithofacies. (b) Line scan and schematic drawing of tuff and clast-supported polymictic lapilli-tuff lithofacies. (c) Fine-grained light green tuff, including: (1) sand-sized tuff with planar stratification, and (2) silt-sized vitric light green tuff with convolute bedding. (d) Photomicrographs of lapillistone and lapilli-tuff (plane-polarized light): 1. Lapillistone dominated by plagioclase-phyric andesite clasts with minor pumice clasts. 2. Lapilli-tuff with pumice clasts and fiamme.

between unconsolidated sediment and sedimentary rock; on this basis the transition lies at 427 mbsf (bottom of Hole U1437B and top of Hole U1437D). Exact positions of the contacts between lithostratigraphic units are given in the work of Tamura *et al*. (2015a, 2015d).

Lithostratigraphic unit I (0–682.12 mbsf)

Unit I is 0 to ~4.3 Ma in age (Figure 9), is 682.12-m thick, and consists largely (88%) of mud/mudstone with 25–75% dispersed ash, referred to as tuffaceous mud or mudstone (depending on whether or not it is lithified; Figures 10 and 11). The tuffaceous mud/mudstone contains abundant fine colourless glass shards and rare crystals, plus carbonate materials such as foraminifers. The rest of unit I (12%) consists of ash or tuff intervals (again depending on whether or not it is lithified), except for very rare (1.2%) lapli-ash/lapilli tuff and lapillistone intervals with pumice or scoria <1 cm in size. The ash/tuff lithofacies was mainly differentiated
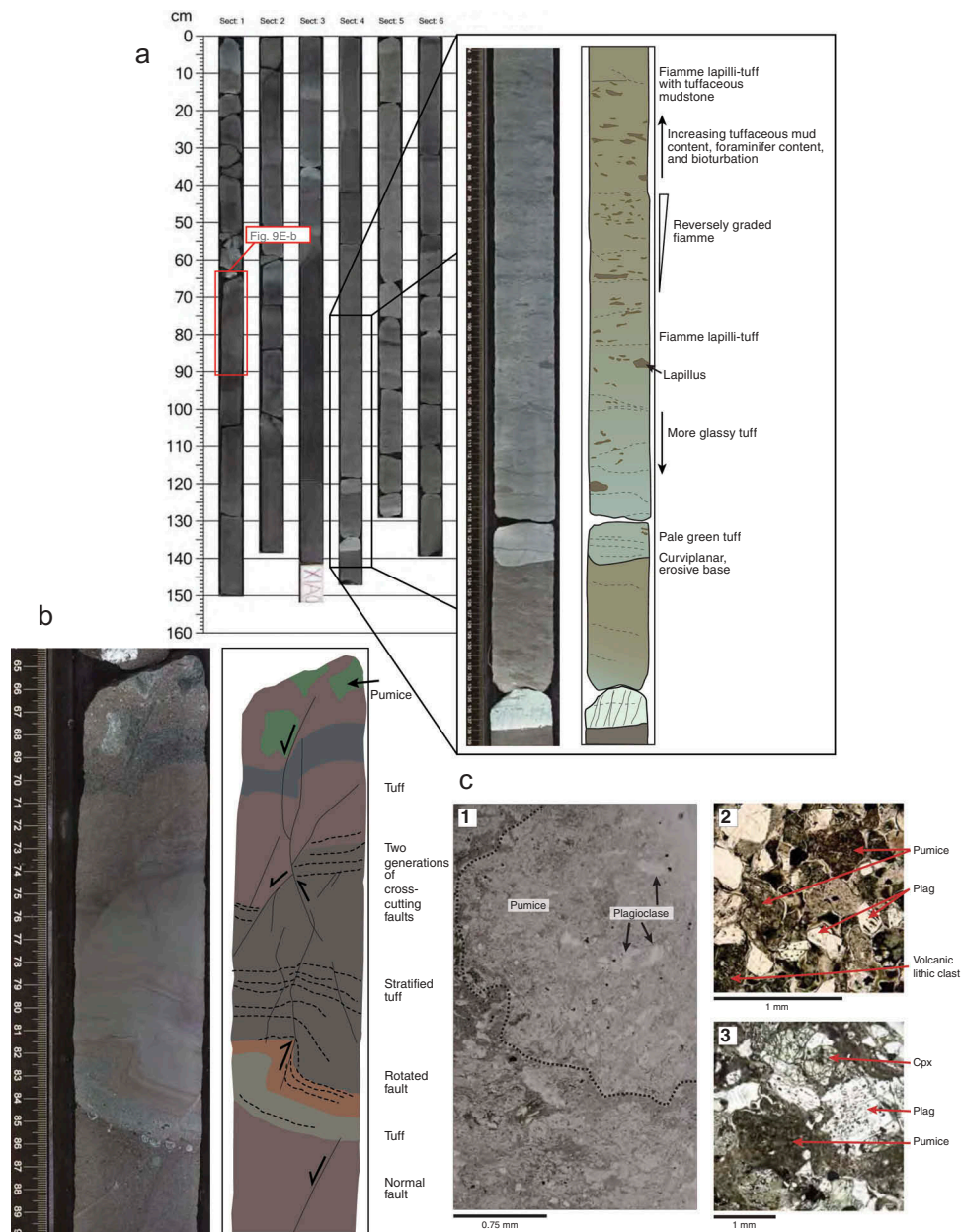
Figure 15. Unit V. (a) Monomictic reversely graded lapilli-tuff with tuffaceous mudstone. The lapilli are made of flattened pumice (fiamme) or nonflattened pumice. Note the erosive base and reverse coarse-tail grading of lapilli, with upward-increasing tuffaceous mudstone. (b) Annotated line scan of soft-sediment faulting in tuff, unit V. (c) Lapilli-tuff and lapillistone: (1) white to light grey lapilli-tuff with large pumice lapillus. The matrix is composed of glass shards, smaller pumice lapilli, and plagioclase; (2) clast-supported dark grey-green lapilli-tuff showing pumice lapilli and volcanic lithic clasts, plagioclase, and opaques; (3) clast-supported dark grey-green lapilli-tuff with crystals of pyroxene, plagioclase, and opaques; the large feldspars have visible melt inclusions.

into two types, evolved (white to dark grey, probably intermediate to silicic composition), or mafic (black, with brownish shards). A small number of intervals were described as bimodal because they have both colourless and brown-coloured glass. The ashes/tuffs are mainly composed of glass shards (i.e. they are vitric tuffs), although some are graded, with crystal-rich basal layers, commonly plagioclase and pyroxene (Figure 11). Sedimentary structures include lamination and

bioturbation (Figure 11). Evolved ash/tuff intervals are four times as common as the mafic ash/tuff intervals. Hornblende-bearing evolved ashes/tuffs, while rare (7%), have elevated K_2O contents relative to most of the other ash/tuff intervals (geochemical methods described in Tamura *et al.* 2015b); we suggest these record rear-arc seamount volcanism rather than arc front or rift volcanism (geochemistry discussed further later). Unit I has an unusually high sedimentation rate
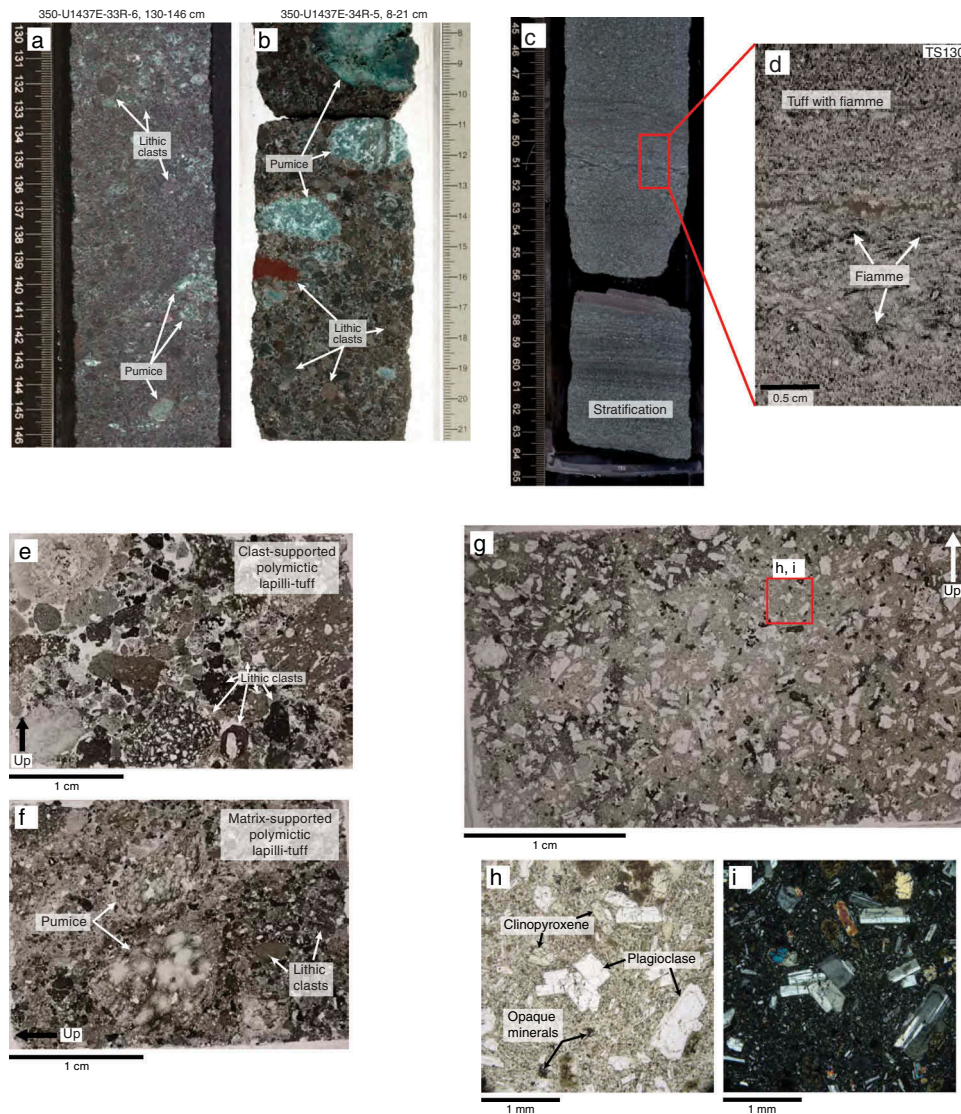
Figure 16. Unit VI. (a) Clast-supported polymictic lapilli-tuff with subrounded pumice and lithic clasts of rounded mafic and evolved volcanics. (b) Clast-supported polymictic lapillistone with pumice and lithic clasts of subrounded tuffaceous mudstone and evolved volcanics. (c) Stratification in a tuff layer with subordinate fiamme, in macroscopic view, and (d) in microscopic view. (e) Microscopic view of clast-supported polymictic lapilli-tuff. (f) Microscopic view of matrix-supported polymictic lapilli-tuff. (g) Andesite clast with plagioclase, clinopyroxene, and opaques (plane-polarized light). Red box = location of photomicrographs shown in (h) plane-polarized light and (i) cross-polarized light.

for fine-grained deep marine sediment far from a continental margin and not associated with a deep-sea fan system; it is ~118 m/million year in the upper 230 m (0–2 Ma), and ~200 m/million year in the lower 450 m (2–4.3 Ma).

For more than 4 million year, this part of the Enpo-Manji basin collected mud with a high ash component at a high rate, with volcaniclastic intervals consisting almost entirely of ash/tuff limited to only 12% of the section. The sparseness, thinness, and fine grain size of discrete volcaniclastic layers in lithostratigraphic unit I is enigmatic, given that it accumulated in close proximity to volcanoes of the active rift and back-arc knolls

extensional zone (<3 Ma) and rear-arc seamount chains (>3 Ma), in addition to lying within 90 km of the arc front (Figures 1 and 3). The lateral continuity of reflectors in Lithostratigraphic unit I on the seismic section that lies transverse to the Enpo-Manji basin (Figure 8(c)) is typical of fine-grained basinal deposits far from volcanic sources. Based on features of the volcaniclastic intervals (evolved ash/tuff and mafic ash/tuff), including sharp basal contacts, good sorting, and normal grading, we suggest deposition by suspension settling through water, or by seafloor-hugging density currents, or some combination (e.g. vertical density currents that transition into lateral density currents when they reach the
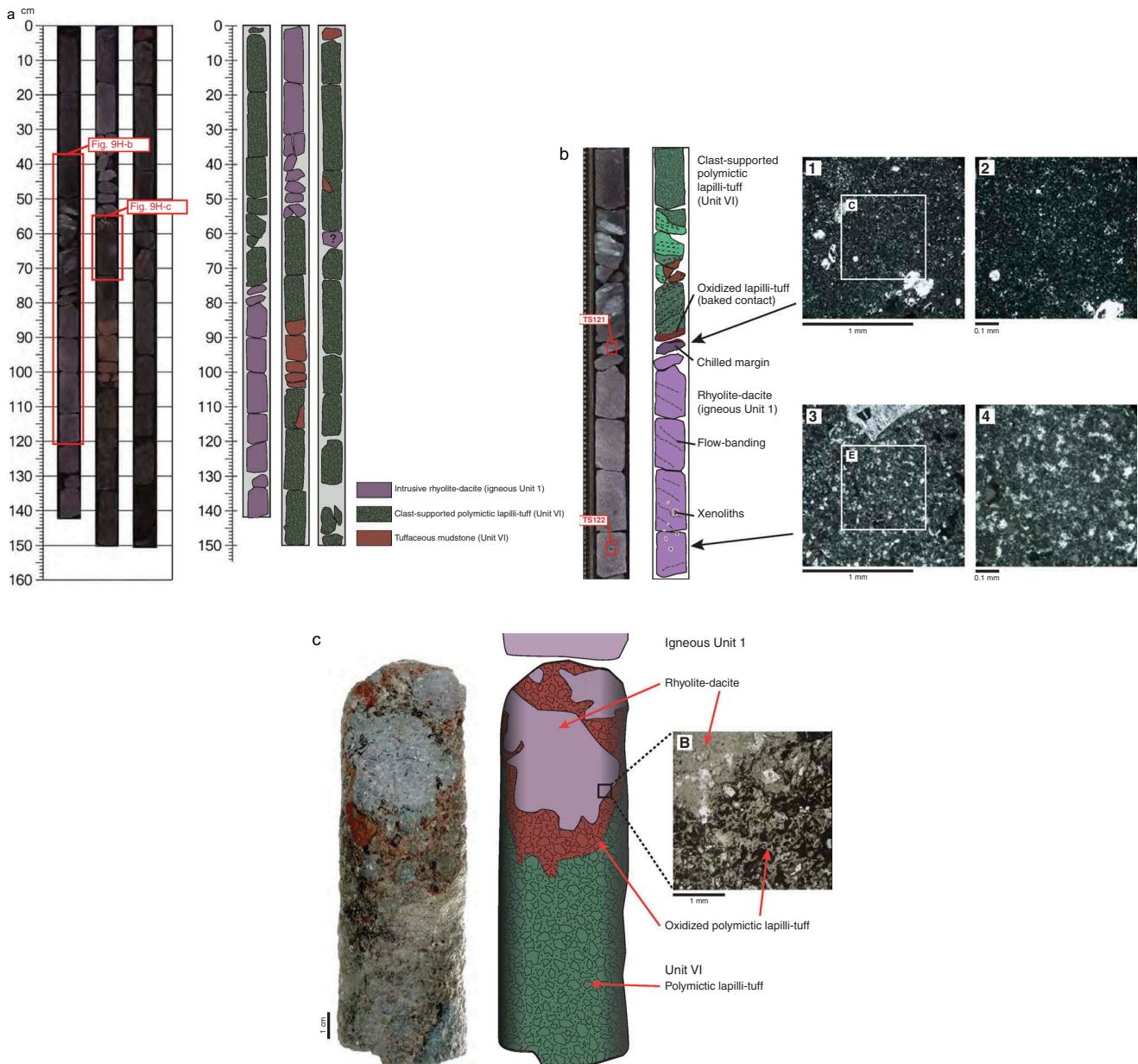
Figure 17. Igneous unit I intrusive rhyolite: (a) Igneous unit I and its intrusive relationship with unit VI. Only 1.21 m was recovered but its true thickness may be up to 6.50 m (see text). A second interval of similar material lower in the core (labelled '?') is only 5-cm thick and has no recovered contacts; it was, therefore, described as a clast (note that similar clasts are described from the host unit VI). (b) Upper contact on igneous unit I intrusive rhyolite and relationship with its unit VI host; for discussion, see text. Photomicrographs of the (1, 2) margin and (3, 4) interior show the chilled upper margin of igneous unit I. (c) Peperitic lower contact on igneous unit I intrusive rhyolite.

seafloor, in a manner envisioned by Carey 1997; Manville and Wilson 2004). Thus, the ash/tuff intervals may represent ash falls from relatively distal subaerial eruptions, which settled through water, and perhaps in some cases flowed along the bottom as dilute density currents, and escaped reworking by bottom currents before burial. The depositional process for the tuffaceous mud/mudstone that make up 88% of unit I is less well understood; it may be hemipelagic rain, dilute

turbid flow, sediment drift, or some combination thereof.

Lithostratigraphic unit II (682.12–726.50 mbsf)

Unit II is ~4.3–4.4 Ma in age and is only 44.38-m thick (Figures 9 and 10), but it makes bright reflectors on the seismic profiles (Figure 8(c,d)). This is because it has much more abundant volcaniclastics (~75%) and much less tuffaceous mudstone (~25%) than is present in units I or III. Additionally, the volcaniclastics in unit II
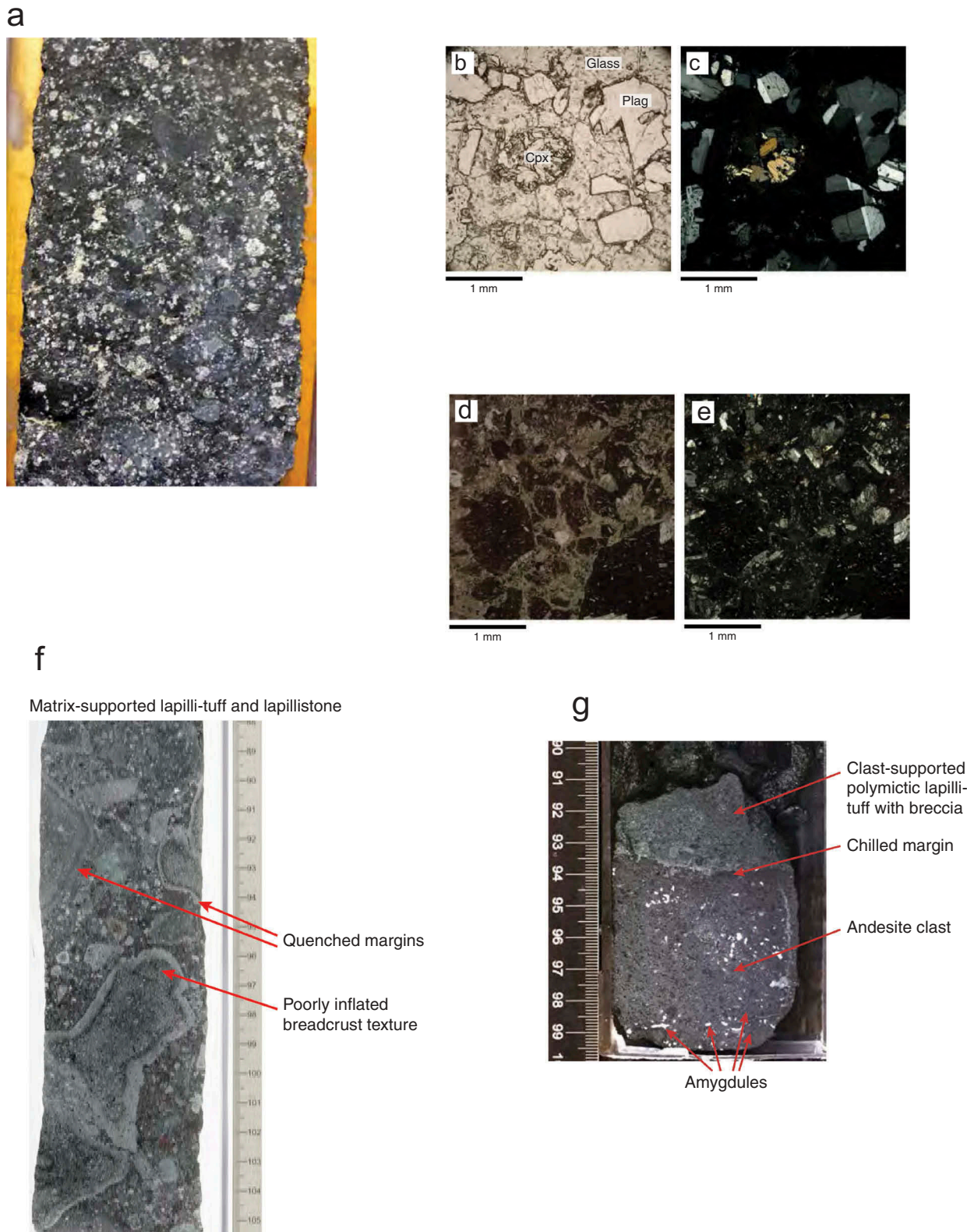
Figure 18. Unit VII: (a) Representative photo of 84-m thick nongraded, nonstratified, black glassy lapillistone and lapilli tuff: consists of nonvesicular glass particles with plagioclase and pyroxene phenocrysts and glomerocrysts, with no bubble-wall shards or broken crystals. (b) Plane-polarized light and (c) cross-polarized light photomicrograph of andesite clast containing plagioclase (Plag) and clinopyroxene (Cpx) in a glass groundmass. (d) Plane-polarized light and (e) cross-polarized light photomicrograph of jigsaw-fit and randomly distributed andesite glassy clasts with poorly inflated breadcrust textures. (f) Matrix-supported lapilli-tuff showing clasts with quenched margins and breadcrust texture. (g) Chilled margin around amygdaloidal andesite lithic clast surrounded by lapilli-tuff.

are coarser grained than those in adjacent units I and III (Figure 12), with pumice lapilli-tuff and pumice lapillistone forming slightly more than half of the thickness, and tuff forming slightly less than half. The volcaniclastics in unit II also differ from those of units I and III by being entirely evolved (no mafic volcaniclastics present). The volcaniclastic intervals are planar bedded or cross bedded, and commonly show normal grading (Figure 12). They contain plagioclase, clinopyroxene, orthopyroxene, and amphibole crystals in varying proportions. The tuffaceous mudstone is like that of unit I but more lithified and altered to green clay minerals.

Unit II is dominated by monomictic pumice lapilli-tuff and lapillistone that is relatively well sorted, with abundant interstratified well-sorted crystal and vitric tuff, and is stratified, with planar and cross lamination, sharp bases, and graded bioturbated tops (Figure 12). We interpret it to represent the deposits of density current deposits, and the monomictic composition may indicate that at least some were eruption fed.

Lithostratigraphic unit III (726.50–1017.88 mbsf)

Unit III is ~4.4–6.2 Ma in age (Figure 9), is 291.38-m thick, and is dominated by tuffaceous mudstone (~64%) and lesser tuff (~35%) (Figures 10 and 13). Lapilli-tuff represents only ~1% of the unit. All intervals of tuff, and the rare lapilli-tuff, are compositionally evolved. Unit III shows an increase in fine-grained tuff (relative to tuffaceous mudstone) in its basal ~80 m; above that, unit III is similar to unit I, except that it lacks the mafic tuff that makes up ~20% of the tuff in unit I. The tuffaceous mudstone intervals in unit III have abundant bioturbation (Figure 13). The evolved tuffs of unit III are of two main types: (1) dark grey tuffs identical to those of units I and II, and not described further here; and (2) intercalated white to grey-green tuff, which is much finer grained and better sorted, in places appearing chert-like, i.e. a dense very fine-grained siliceous material (Figure 13). This fine-grained tuff has laminations produced by alternation of glass shard–rich layers (white) and layers of mixed shards, pumice, and crystal fragments (grey-green), repeated over intervals up to several meters thick, with no bioturbation or tuffaceous mudstone interbeds. Thus, the intervals seem to record fairly continuous but pulsating sedimentation, probably from unsteady density currents, over a relatively short period of time for each interval (possibly days or weeks). The laminations commonly show soft-sediment deformation (Figure 13), supporting the interpretation that the intervals were deposited rapidly. Intercalated white to grey-green evolved tuff intervals form much of the volcaniclastics in the lower part of unit III, where the volcaniclastic content is highest for this unit. The very large quantity of very fine glass shards in this facies suggests phreatomagmatic eruption, typified by extremely efficient glass fragmentation due to enhanced explosivity (Fisher and Schmincke 1984). This lithofacies also occurs in units IV and V.

Unit III also contains one distinctive interval (1.91-cm thick) with deformed tuffaceous mudstone intraclasts (up to ~20 cm in size) and clasts of scoria and pumice (up to 5 cm) supported in a deformed tuffaceous mudstone matrix; this is interpreted to represent a disaggregated slump or submarine debris flow deposit.

Lithostratigraphic unit IV (1017.88–1120.11 mbsf)

Unit IV is ~6.2–7.5 Ma in age (Figure 9), and is 102.23-m thick (Figure 10). It contrasts with the tuffaceous mudstone-dominated units III and V, and consists of four lithofacies, in order of abundance: (1) normally graded polymictic lapilli-tuff and lapillistone (Figure 14). Lapilli are small (average 3–5 mm), and volcanic lithic clasts dominate over pumice, and are plagioclase-pyroxene andesites (Figure 14), that is, they are evolved. Shell fragments are also present, indicating that at least some of the material was sourced from shallow water. (2) Intercalated white to grey-green evolved tuff, identical to that in unit III (compare Figure 14(c) with Figure 13(b)). Similarly, it forms multi-metre thick, non-bioturbated intervals with planar lamination or soft-sediment deformation. (3) Dark grey evolved tuff, like that described in units I, II, and III, with plagioclase, pyroxene and pumice. (4) Tuffaceous mudstone, like that described in units I, II and III. For interpretation of the second through fourth lithofacies, see above. The first lithofacies (polymictic, evolved lapilli-tuff and lapillistone) occurs as very thick (multimetre) relatively well-sorted intervals with no internal stratification, composed of volcanic clasts of a variety of evolved types (Figure 14(a,b)). These characteristics suggest deposition from high-concentration density currents, probably by mass wasting or resedimentation from one or more volcanoes; alternatively, this facies could be products from pyroclastic eruptions that mobilized large volumes of lithic clasts. This lithofacies is also abundant in unit V.

Lithostratigraphic unit V (1120.11–1320.00 mbsf)

Lithostratigraphic unit V is ~7.5–9 Ma in age (Figure 9), and is 199.89-m thick (Figure 10). It is distinguished largely on the basis of its intervals of monomictic reversely graded pumice lapilli-tuff (Figure 15(a)); these distinctive beds, with their flattened pumice and nonflattened pumice dispersed in a tuff matrix, contrast with the polymictic, dominantly lithic lapilli-tuff of the overlying and underlying units (IV and VI). The flattened pumice is referred to as 'fiamme' with no connotation of welding compaction; in fact most or all of the pumices were probably flattened during diagenesis.

Each monomictic reversely graded pumice lapilli-tuff in unit V has (Figure 15(a)): (1) a sharp base, typically eroded into the underlying tuffaceous mudstone, overlain by (2) evolved tuff with abundant glass shards and grains of pumice, in turn grading upward into (3) pumice lapilli-tuff with flattened or non-flattened pumices that become progressively coarser upward (i.e. reversely graded); this passes upward into (4) tuffaceous mudstone. This lithofacies is thus composed almost entirely of vitric material (glass shards and pumice). This monomictic tuff with pumice and fiamme makes up 13% of unit V and recurs throughout. We interpret this lithofacies to represent density current deposits, based on (a) basal scours; (b) poor sorting with ash-sized material with pumice lapilli or fiamme that become more abundant upward in each bed, indicating density grading; and (c) the increase in tuffaceous mudstone at the top of each bed. The monomict composition and the presence of abundant evolved glass shards, pumice, and broken crystals indicate that these were fed from pyroclastic eruptions.

Similar to units I, III, and IV, unit V also has tuffaceous mudstone (69%); evolved tuff (15%), some with soft-sediment faulting (Figure 15(b)); and lapilli-tuff and lapillistone (3%) with lithic and volcanic rock fragments (Figure 15(c)).

Lithostratigraphic unit VI (1320.00 to 1459.80 mbsf)

Lithostratigraphic unit VI is older than ~9 Ma (Figure 9) and extends to at least 10.97–11.85 Ma in age, and is 139.80-m thick (Figure 10). It is characterized by an abundance of polymictic lapilli-tuff with pumice and lithic clasts (Figure 16(a,b)), although it also contains monomictic pumice lapilli-tuff (Figure 16(c,d)). The top of lithostratigraphic unit VI is marked by the first appearance of multiple intervals of polymictic lapilli-tuff, and its base is marked by the top of a very distinctive black monomictic glassy lapillistone and lapilli-tuff in the upper part of unit VII.

The polymictic lapilli-tuff and lapillistone forms very thick beds (>1.5 m, the length of a core section, or up to 2.8-m thick assuming complete recovery between core sections). Tuff and tuffaceous mudstone intervals are interbedded. Polymictic lapilli-tuff with pumice and lithic clasts is four times more abundant than monomictic pumice lapilli-tuff in unit VI; monomictic varieties contain only pumice, whereas polymictic varieties have evolved and lesser mafic volcanic lithic clast types as well as pumice clasts (Figure 16(a,b)). The polymictic lapilli-tuff with lithic clasts and pumice shows a complete gradation from clast-supported (Figure 16(e)), to matrix-supported (Figure 16(f)) whereas the monomictic pumice lapilli-tuff is entirely matrix-supported.

Lithic lapilli in unit VI are dominantly:

• Porphyritic andesite with plagioclase and clinopyroxene (Figure 16(g–1)). Clasts of this type also occur as scattered small blocks (>6.4 cm in size) in the polymictic lapilli-tuff.

• Rhyolite-dacite, which becomes more common near the rhyolite intrusive sheet with peperitic boundaries, described as igneous unit I in the following. These include crystal-poor and porphyritic varieties, with amphibole, plagioclase, and quartz.

Pumice lapilli clasts in unit VI are light to dark green and commonly flattened by compaction and lithification into fiamme (Figure 16(c,d)). Red to brown tuffaceous mudstone clasts are also present in unit VI (Figure 16(b)).

In summary, unit VI is dominated by lapilli-tuff and lapillistone in very thick (multimeter) beds with no internal stratification, composed of volcanic clasts of a variety of evolved types (Figure 16(a,b)); this was deposited from high-concentration density currents, probably by mass wasting or resedimentation from one or more volcanoes. Additionally, unit VI has matrix-supported monomictic pumice lapilli tuff that may have had been fed from pyroclastic eruptions.

Igneous unit I (1388.86–1390.07 mbsf)

The only igneous unit at Site U1437 consists of a single rhyolite intrusion, which lies within lithostratigraphic unit VI (Figure 10). As noted above, igneous unit I yielded a U–Pb zircon age of 13.6 Ma ±1.7 in shore-based work immediately following the expedition, described by Konrad et al. (2016). Core recovery is much lower in igneous unit I (~45%) than its host volcaniclastic rock (~94%), and the recovered igneous unit I core material is fractured by drilling disturbance (Figure 17), probably due to greater competency of the rhyolite intrusion compared to the surrounding volcaniclastic host. Therefore, although only 1.21-m thickness was described for igneous unit I (Figure 17), its maximum thickness is estimated at 6.50 m assuming all the material not recovered from this interval was part of igneous unit I.

Shipboard geochemical analysis (discussed later) shows that igneous unit I is a rhyolite with 74.5% SiO_2. It has sieve-textured subhedral plagioclase (up to 4 mm, ~7%), euhedral hornblende (up to 0.5 mm, ~3%), large anhedral to subhedral quartz (up to 8 mm, ~1%) with fresh glassy melt inclusions, some opaque minerals, and rare zircon (<30 μm in size). Flow banding is observed across the entire unit in various orientations (Figure 17(b)). The groundmass varies from cryptocrystalline near the upper and lower contacts to fine grained in the centre of the unit (Figure 17(b)). Palaeomagnetic data on igneous unit I show a consistent, single component demagnetization and normal

polarity with appropriate inclination of the characteristic remanent magnetization, supporting the interpretation that igneous unit I is an intrusion, rather than simply a large clast. The upper margin of the intrusion is chilled, and the overlying lapilli-tuff is baked (Figure 17(b)), also indicating that igneous unit I is an intrusion rather than a clast or lava. The lower contact of igneous unit I is peperitic, defined as a magma-wet sediment mixture (Busby-Spera and White 1987); the contact shows complex mingling between the intrusion and the host, including crenulated lobate margins on the intrusion and dispersal of the magma into the host on the microscopic scale (Figure 17(c)). Peperite is considered penecontemporaneous with the section it intrudes (Busby-Spera and White 1987). Blocks of similar material occur in the host, unit VI (rhyolite-dacite blocks, described earlier), indicating that the body locally vented onto the surface during accumulation of unit VI.

Lithostratigraphic unit VII (1459.80–1806.50 mbsf)

Unit VII is older than 10.97–11.85 Ma and is 346.70-m thick (Figure 10). It is ~90% extremely thick bedded, nongraded, nonstratified, poorly sorted, coarse-grained angular andesitic lapilli-tuff, in places with blocks tens of centimetres in size (Figure 18). Some of these blocks have quenched margins, jigsaw-fit textures, intricate fluidal margins, or peperitic margins, described in detail later. These features indicate that the blocks were emplaced hot, so the blocks could have originated as hot clasts, lava, and/or intrusions. Thus unit VII is interpreted to be a near-vent deposit. Unit VII is divided into upper and lower parts (shallower and deeper than 1643.73 mbsf).

Upper part of unit VII: black glassy lapillistone and lapilli-tuff

The upper part of unit VII consists of one massive (nonstratified) ~184-m thick deposit of homogeneous, nonvesicular glassy black lapillistone and lapilli-tuff. The glass clasts are unaltered and angular, with abundant large clinopyroxene glomerocrysts and plagioclase glomerocrysts (Figure 18(a)). The glass is isotropic and nonvesicular, and bubble-wall shards or broken crystals are absent (Figure 18(a,c)). Only a few volcanic lithic clasts are present, some with quenched margins, and a few red oxidized clasts also occur. The black glassy lapillistone and lapilli-tuff lithofacies lacks stratification completely, except for one thin (~25-cm thick) interval of crudely stratified ash. The angular, glassy, nonvesicular, monomict character of the clasts, together with the lack of bubble-wall shard or broken crystals, indicates fragmentation by autobrecciation and quenching of lava in a submarine environment (i.e. hyaloclastite). The few nonglassy clasts in the deposit suggest minor accidental incorporation of clasts during transport, but most of the unit is monomictic and nonstratified, indicating minimal resedimentation. A lack of tuffaceous mudstone interbeds indicates rapid accumulation.

Lower part of unit VII: coarse-grained massive lapilli-tuff with in situ quench-fragmented blocks

The lower part of unit VII (~157-m thick) is dominated by a lithofacies of green (i.e. altered) angular andesite lithic lapilli-tuff, in places with blocks up to 53 cm in size (tuff breccia) (see Figure 18(f,g)). Like the black glassy lapillistone and lapilli-tuff unit that forms the upper part of lithostratigraphic unit VII, these lithic lapilli-tuff and tuff-breccia intervals are massive, forming extremely thick intervals of nonstratified, very poorly sorted monomictic andesite lapilli-tuff with blocks, but unlike the upper part of unit VII, the lower part has intercalated stratified lithic lapilli-tuff and tuff (also altered green). Clasts in the extremely thick nonstratified intervals are angular or have very irregular shapes, including jig-saw fit clasts (Figure 18(d,e)), indicating very minimal transport. Many intervals contain glassy blocks and coarse lapilli, and some have glassy rims and poorly inflated breadcrust or cauliflower texture, indicating that clasts came to rest at high temperatures (Figure 18(f,g)). In at least one case, a clast appears to be surrounded by sediment with a baked margin. Additionally, there are no clasts with broken chilled margins as would be expected if the clasts were transported and deposited after they cooled. In some intervals, very angular, jigsaw-fit hyaloclasts (formed of quenched glass) indicate in situ mixing of hot clasts and/or intrusions with the host hyaloclastic tuff-breccia, all of the same andesitic composition. On the basis of the core, it is not possible to determine whether all of these features formed on hot clasts or if some of these features formed on the complexly embayed margins of small intrusive bodies or lava. Further support of hot emplacement is provided by palaeomagnetic inclinations from two of the clasts; despite multidomain overprinting, the demagnetization analyses of these two individual clasts resolved the characteristic reversed polarity expected for hot emplacement (for more details see Tamura et al. 2015a). Some intervals have more heterogenerous andesite lithic clast types, with variable plagioclase and pyroxene contents, and

ranging from nonvesicular to moderately vesicular, indicating resedimentation.

Petrophysical data from cores and downhole logging

We collected petrophysical data from all cores, including density and porosity, sonic velocity, magnetic susceptibility and natural gamma radiation (Figure 19). In addition, we conducted downhole logging operations in Hole U1437D, from 92 to ~960 mbsf. The logging parameters included those measured on Figure 19, plus bulk resistivity, and micro-resistivity imaging (not presented here).

The top 92 m could not be logged because the drill pipe extended to that depth for operational and safety reasons. The logs extend to ~960 mbsf because 980 mbsf was the depth of the hole when the drill string had to be retrieved for a bit change and it seemed prudent to conduct a first set of downhole measurements at that time. After logging was completed, Hole U1437D was deepened from 980 to 1105 mbsf, where drilling difficulties were encountered and the hole had to be terminated. We drilled a new Hole U1437E to that depth without coring, deployed a 1086-m long casing string, and cored from 1104 to 1806 mbsf. At that time a technical problem precluded re-entry and we could not log Hole 1437E. Fortunately the on-board
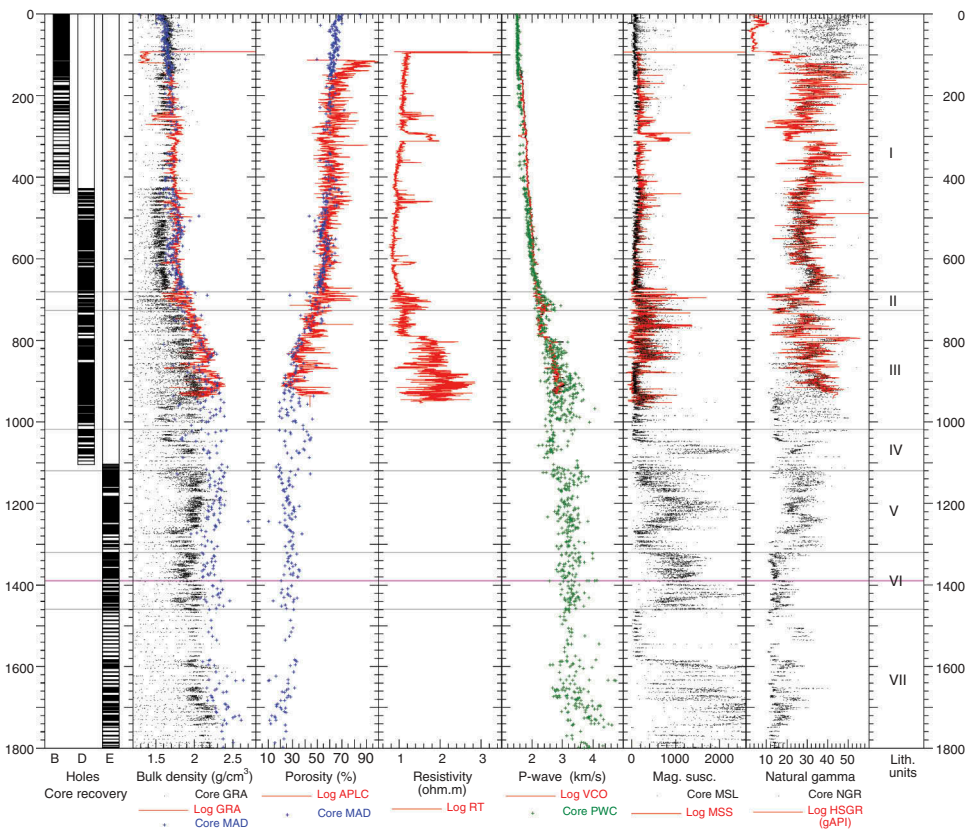
Figure 19. Petrophysical data from cores (whole-round core section logging, black dots; section half measurements, green crosses; discrete samples, blue crosses) and from downhole logging (red lines). Three holes were cored at Site U1437 (B, D, E) with core recovery shown in the left-most column (black = recovered, white = not recovered). GRA = gamma ray attenuation method. PWC = P-wave caliper method. MAD = moisture and density method. Log RT = 'true resistivity' from downhole logging. Mag. Susc. = magnetic susceptibility. Bulk density estimates from the MAD method used on cores match very well the values obtained with the GRA method in downhole logs. Density values using GRA on cores (black dots) are underestimated because (1) calibration is routinely performed for 66 mm diameter cores (as in Hole U1437B) and not the 58 mm diameter cores of Holes U1437D and E; and (2) core disturbance (gaps, cracks, washouts) result in even lower values. These data are useful for the detection of core disturbance and they can be partially corrected for a high-resolution density record with some effort. Porosity and P-wave velocity values obtained from cores and from logs match well despite the different methods, tools and scales employed. Magnetic susceptibility values are arbitrary instrument units from both core and downhole detectors and we bring the values to the same scale by multiplying the log values with 10^5 and adding 30. Natural gamma radiation values from cores are in instrument-specific counts/s unit, whereas those from downhole logs are calibrated according to the American Petroleum Institute (API) standard and expressed as gAPI. We chose to bring the core and log records to the same scale by multiplying the core data by 1.4 and adding 8. Technical difficulties prohibited downhole logging in Hole U1437E. Grey lines delineate lithologic unit boundaries (Roman numerals in Lith. Units column). Purple lines (appear as one line) represent the nominally 1.2-m thick igneous unit I.

petrophysical measurements were unaffected (Figure 19). The two shallowest logging unit boundaries, between 1 and 2 and between 2 and 3, correspond to the lower boundaries of sharp resistivity anomalies at 310 and 612 m, respectively, and both lie within lithologic unit I. Logging unit boundary 3–4 corresponds to lithologic unit boundary I/II at 680 m. The lower boundary of the conspicuous lithologic unit II was not defined in the logging data, although it can be clearly recognized in the resistivity log. The deepest logging unit boundary 4/5 at 789 m corresponds to an increase in natural gamma radiation and resistivity and lies within lithologic unit III (Figure 19).

The first order trends in physical properties are indicated by density, porosity, resistivity and p-wave velocity. These all change rapidly with depth in the interval ~700–950 mbsf, which corresponds to lithologic unit II and most of unit III. The trends above and below this interval have similar and lower rates of change with depth; the range of values is significantly larger below 950 mbsf.

The higher rate of downhole increase in density and sonic velocity, and the corresponding decrease in porosity, in the interval 700–950 mbsf, are the result of compaction and cementation by incipient diagenesis in the volcaniclastics and tuffaceous mudstone of lithologic units II and III. These trends are accompanied by significant changes in the magnetic susceptibility (MS) and natural gamma radiation (NGR), which are compositional proxies. MS is low in the upper 700 m at Site U1437, increases two to threefold in the interval 700–950 mbsf, and below 950 mbsf shows a cyclic pattern with values ranging from lowest to highest in the entire section. MS variations most likely reflect oxide concentration, particularly magnetite. NGR, in contrast, has generally higher values above 1000 mbsf and lower values below, suggesting first-order changes in sediment provenance above and below that depth; this lies at the unit III/IV boundary at ~6.2 Ma (Figure 19).

The interval at 290–312 mbsf (logging depth, within unit I, Figure 19) shows a sharp resistivity increase to twice the local baseline value. In the Formation MicroScanner (FMS) micro-resistivity images, this interval appears slightly less layered (more granular or chaotic?) than the overlying and underlying intervals. In this same high-resistivity interval, MS values triple, and natural gamma radiation drops to local minimum values. The corresponding interval in the cores (at coring depth scale) had almost no recovery: Core U1437B-40X (291.1–300.8 mbsf) had 1.8 m recovery (12%) and the recovered tuffaceous mud and ash layers are indistinguishable from overlying sediments. Cored intervals 41–42X (300.8–320.2 mbsf) had zero recovery.

Furthermore, when we attempted to drill Hole U1437C to 425 mbsf without coring, circulation and rotation were lost at 309.7 mbsf. The bit had to be dropped and the stuck pipe had to be worked for several hours before it became free and could be retrieved, at which point Hole U1437C was abandoned. The drilling problems in this interval suggests loose or fractured material, however, that would not explain higher resistivity, which may indicate less porosity (cementation, remolding) or less saline pore water. The high-resistivity interval corresponds to the sequence boundary between seismic layers L2 and L3 (Figure 8), a boundary that may reflect a period of non-deposition, erosion and/or deposition by mass wasting, and/or lateral fluid flow. The MS and NGR signals could indicate a primary compositional change or alteration associated with fluid flow. At this time we simply don't know what this mystery interval represents. An interval with similar log signature at 607.3–614.6 m (logging depth) has also lower, but reasonably good core recovery (~60%, compared to ~82% in 50 m above and ~97% in 50 m below). The recovered material from this interval is tuffaceous mudstone with intercalations of tuff and shows no obvious characteristics that would differentiate it macroscopically from the overlying and underling intervals.

Over the entire section at Site U1437, both MS and NGR records show high-amplitude variations at the decimetre to metre depth scale that can be linked to lithologic and compositional changes. These relationships cannot be elaborated or illustrated within the scope of this overview and are subject to on-going studies.

Interpretation of depositional environment at Site U1437: deep-water basinal succession

As noted above, the section drilled at Site U1437 accumulated in a deep-water volcano-bounded basin between the Manji and Enpo seamount chains. We now present evidence that the section is best described as a deep-water basinal succession, characterized by fine-grained well stratified, laterally continuous deposits in the upper 75% of the section; this passes downward into proximal volcaniclastic deposits in the lower 25% of the section, which we infer records eruption and sedimentation from nearby volcanoes and localized venting within the deep-water basinal setting.

Upper 75% of the section drilled at Site U1437

This part of the section (units I through V; 0–1320 mbsf; ca. 0–7.5 Ma) has the following characteristics:

- It is mostly tuffaceous mudstone (~60%) deposited from hemipelagic rain, dilute turbid flows, bottom currents/sediment drift, or some combination thereof.
- The grain size of volcanic clasts in the discrete volcaniclastic layers is small: about half ash and half fine-grained lapilli.
- Lack of block-sized clasts.
- Little evidence for density current deposits, except in unit II, which is thin; most of the volcaniclastics could represent suspension fallout from distal eruptions.
- There is no geomorphic or seismic stratigraphic evidence for fan- or wedge-shaped sediment bodies or of chaotic facies; instead, the seismic reflection images show laterally persistent tabular stratification, consistent with the fine grained character of the section drilled.

In summary, from 0 Ma to ca. 7.5 Ma, hemipelagic sedimentation dominated the basin, with ash regularly deposited in the area and variably mixed with mud of uncertain origin (possible origins of the mud discussed later). Lapilli-sized fragments (albeit fine-grained) were only provided to the basin in one brief episode at 4.3 Ma, represented by unit II, and it is dominated by evolved pumice lapilli indicative of an explosive volcanic event; however the fine grain size of the lapilli could indicate that the eruption was relatively distal, and this unit only represents 3% of the drilled section. Two aspects of the upper 75% of the section are difficult to explain: (1) The section is much more mud-rich than expected for an arc-proximal sedimentary succession, and (2) the grain size of the volcaniclastics is much smaller than expected for an intra-arc basin surrounded by volcanoes.

Lower 25% of the section drilled at Site U1437

This part of the section (unit VI, igneous unit I, and unit VII; 1320–1804 mbsf; ca. 9–14 Ma) differs from the upper 75% in the following ways:

- Tuffaceous mudstone is minor (10% of unit VI) to absent (unit VII).
- The grain size of volcanic clasts increases dramatically, with coarse-grained lapilli dominating the section, and blocks occurring in unit VII.
- Lapilli-sized volcaniclastics of unit VI are polymictic and formed thick massive beds, some graded; these were deposited from density currents carrying detritus from seamounts surrounding the Enpo-Manji Basin. Intervening minor tuffaceous mudstone record background hemipelagic sedimentation between density current events.

- Andesite lapilli tuff and tuff breccia of unit VII are monomictic, and show macroscopic textural evidence of quench fragmentation and palaeomagnetic evidence of emplacement at high temperatures. The absence of background sediment (tuffaceous mudstone) indicates high/steady volcanic input. Unit VII is a vent-proximal deposit.
- Unit VI was intruded by a quartz-phyric rhyolite-dacite sheet dated at (13.6 + 1.6/−1.7) Ma (igneous unit I); this intrusion is a peperite (formed by mixing of magma and wet sediment), indicating that it formed contemporaneously with the section it intrudes; furthermore, blocks of igneous unit I are scattered through the section above and below, indicating its contemporaneity with unit VI.

In summary, from ~9 to 14 Ma, coarse-grained volcaniclastic sedimentation dominated the area of Site U1437, with polymictic material derived from adjacent volcanoes (unit VI), and monomictic material produced by local eruptions (unit VII) and peperite intrusions (igneous unit I), with little to no evidence for resedimentation, i.e. dominantly *in situ*.

Shipboard igneous geochemistry

This section is brief, because shore-based micro-analytical igneous geochemical studies (in progress) are expected to be much more revealing than the ship-based studies. This is because:

• The fine grain size of the upper 75% of the section largely precluded analysis of individual clasts by shipboard techniques, requiring us to analyse bulk samples, referred to as 'volcaniclastic samples' (Figures 20 and 21), taken from different parts of lapilli-tuff or tuff beds, some of which are graded. Shipboard analyses of individual clasts are restricted to: (1) a single dacite pumice clast from unit II, (2) a single andesitic lithic clast from unit IV. These two clasts, along with igneous unit I, are referred to as 'igneous samples'. Shore-based microanalytical techniques will allow analysis of individual clasts that are lapilli- to ash-sized.

• Due to alteration, shipboard analyses relied largely on Zr, Zr/Y and Zr/Y vs. SiO_2 plots for distinguishing defining geochemical units (Figures 20 and 21). We focused on Zr and Y because they are relatively fluid immobile and remain robust during alteration (Gill *et al*. 1994). We used shipboard Zr/Y analyses as an indicator for magmatic provenance and to distinguish between rear-arc and arc-front sources. Micro-analytical techniques will be more successful at exploiting relict glass domains, and will be used to determine the chemistry of minerals, which are less altered than the glass.
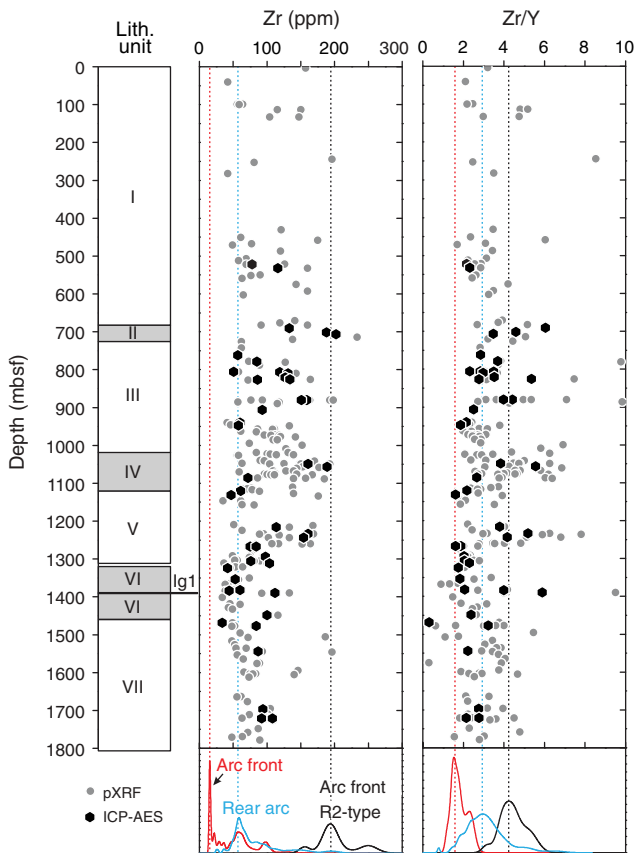
Figure 20. Zr/Y vs. SiO$_2$ for volcaniclastic and igneous samples from sedimentary units I–VII and igneous unit I (Site U1437) (below), compared to literature data from Izu arc and from the Izu arc (above). Literature data include: rear arc volcanoes, shown in blue; arc front basalt-dominated island volcanoes with small volumes of rhyolite (R1 type rhyolite), shown in red; and arc front rhyolite-dominant submarine calderas (R2 type rhyolite), shown in black. R1 and R2 rhyolites defined by Tamura et al. (2009). Literature data sources: Tamura et al. (2009), Gill et al. (1994), Bryant et al. (2003), Straub (2003, 2010), Hochstaedter et al. (2001), Ishizuka et al. (2002, 2003a, 2003b, 2006a, 2006b), Machida et al. (2003, 2008), Tollstrup et al. (2010). Samples from units I through V (upper 1320 m) lie in both the arc front and rear arc fields, consistent with their fine grain size, which may be distal from sources. In contrast, units VI and VII (lower 25% of section) are coarse-grained, vent-proximal deposits (see text), and igneous unit I is an intrusion and thus also vent-proximal; however, these plot mainly in the arc front field, despite their position in the rear arc. This suggests that rear arc magmas only fully compositionally diverged after ca. 13 Ma. (Note: one outlier contains anomalously high Zr/Y and is not included in the fields.) Figure reprinted from Proceedings of the International Ocean Discovery Program, Expedition 350 (Tamura et al. 2015a) with permission from IODP.

Downhole geochemical variations in units I–V generally reflect the relative proportions of distal arc-front and proximal rear-arc volcanic sources (Figure 21). As a general trend, coarse-grained volcaniclastics from units II and IV show stronger rear-arc affinity compared to fine-grained tuff from units I, III, and V. Complications for provenance arise from mixing evident by mafic and
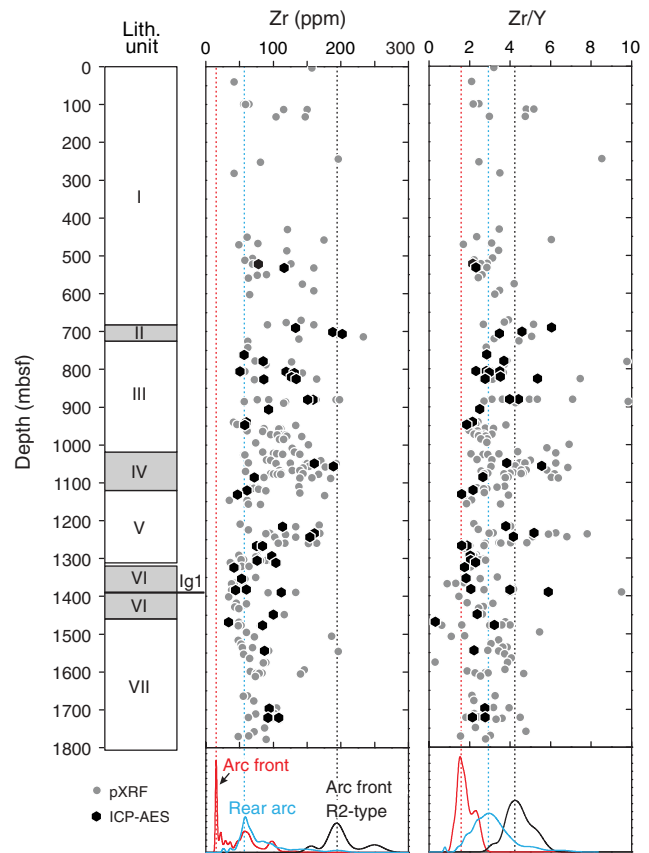
Figure 21. Zr and Zr/Y analysed by pXRF and ICP-AES for volcaniclastic and igneous samples, Site U1437. Probability curves below depth panels show the relative distribution of Zr and Zr/Y in basalt-dominant island volcanoes from the arc front (including R1 rhyolites), rhyolite-dominant submarine calderas in the arc front (R2 rhyolites), and rear-arc volcanic rocks. Vertical lines = composition of the peaks in the literature data distributions. Ig1 = igneous unit I. Data sources: Tamura et al. (2009), Gill et al. (1994), Bryant et al. (2003), Straub (2003, 2010), Hochstaedter et al. (2001), Ishizuka et al. (2002, 2003a, 2003b, 2006a, 2006b), Machida and Ishii (2003, 2008), Tollstrup et al. (2010). Figure reprinted from Proceedings of the International Ocean Discovery Program, Expedition 350 (Tamura et al. 2015a) with permission from IODP.

evolved glass shards in fine-grained volcaniclastic samples. Also, alteration is pervasive in units III and V. The predominance of ash layers from unit I containing low K$_2$O relative to SiO$_2$ indicates a likely arc front or active rift (<1 s Ma) provenance. Volcaniclastics in unit I with high Zr/Y could be mixtures of mafic ash from arc front basalt-dominated island volcanoes, and evolved ash from the rhyolite-dominated submarine calderas (R2 rhyolites), which have high Zr/Y; however, this cannot be confirmed without onshore in situ analyses of glass. The coarse-grained deposits from units II and IV indicate proximal sources. Active Manji seamount chain volcanoes around the time of deposition of unit II (4.2–4.3 Ma) were the Meireki Seamount (3.76 Ma;

Ishizuka *et al*. 1998) ~20 km to the north and the Daigo-Nishi-Aogashima Knoll (5.05 Ma; Ishizuka *et al*. 2003b) ~40 km to the northeast of Site U1437 (Figure 7). Both are rhyolite volcanoes with similar SiO_2 contents (72–76 wt%), whereas Meireki Seamount volcanic rocks have higher K_2O (~3 wt%) but lower Zr/Y (~2.8) compared to the Daigo-Nishi-Aogashima Knoll (K_2O = ~ 1.5 wt%; Zr/Y = ~ 4.4) (Hochstaedter *et al*. 2001). Although the limited data (five analyses in total) available for both seamounts preclude reliable geochemical matching with unit II volcaniclastics, they are potential sources for lapilli in unit II considering their geographic locations, ages, and chemical composition. Similarly, single clast compositions of unit IV can be tentatively matched to available data for Manji Seamount volcanic rocks (Figure 7; ~6.5–6.9 Ma; Ishizuka *et al*. 2002). Two high-K_2O volcaniclastics resemble the high-K Manji Seamount rocks with potassic alteration, whereas most volcaniclastics from unit IV follow the trend for altered Manji Seamount rocks (Ishizuka *et al*. 2002), including depletions in CaO with increasing SiO_2 (see Figure F44 of Tamura *et al*. 2015a). Unit V is primarily tuffaceous mudstone, and given the pervasive alteration throughout this unit, it is difficult to provide an accurate provenance for its volcaniclastic intervals.

The geochemistry of samples from units VI and VII and igneous unit I does not fall neatly into the rear-arc field, but instead spans both fields (Figure 20), even though a rear-arc source is demanded by the vent-proximal nature of the deposits (described earlier). One of the goals of Expedition 350 (Tamura *et al*. 2013) was to determine the timing of development of geochemical asymmetry between the arc front and rear arc. This is important because dredge samples that were already in hand from Neogene volcanoes of the rear arc were more 'continental' in chemical composition than dredge and drill core samples from the arc front, therefore making the rear arc more suitable as a possible building block for continental crust. We presented two models for the development of arc asymmetry: 'from the beginning' and 'from the middle' (Tamura *et al*. 2013). The 'from the beginning' hypothesis stipulated that arc asymmetry was established at Eocene arc inception and persisted through the Neogene. The 'from the middle' hypothesis stipulated that the asymmetry developed during an arc hiatus associated with opening of the Shikoku backarc basin at 27–17 Ma. On the basis of seismic stratigraphy, we expected to reach Oligocene (>23 Ma) strata at 1250 mbsf, to determine which hypothesis was correct, but instead those strata are 9 Ma (late Miocene; lower part of unit V), so the chemistry of the Palaeogene rear

arc remains unknown. However, the compositional heterogeneity of units VI and VII suggests that arc asymmetry did not develop until after ~13 Ma (middle Miocene), which is *during* the Neogene, that is, neither 'from the beginning' nor 'from the middle'.

Depositional model

The biggest surprise of the expedition was the predominance of tuffaceous mud and the fine grain size of the volcaniclastics at Site U1437. We expected to drill into a volcaniclastic apron (see Scientific Prospectus; Tamura *et al*. 2013), with abundant large lapilli- to block-sized volcanic clasts that could be geochemically analysed individually on the ship. This is not what we encountered, but before presenting the depositional model, it is necessary to define the term 'volcaniclastic apron' in order to show how the depositional model for Site U1437 differs from models for volcaniclastic aprons.

Although some may use the term 'volcaniclastic apron' to loosely refer to any accumulation of sediment around a volcano or chain of volcanoes, the term has been used in a much more rigorous sense by sedimentologists over the past 40 years (Karig and Moore 1975b; Sample and Karig 1982; Carey and Sigurdsson 1984; Farquharson *et al*. 1984; Fisher 1984; Busby-Spera 1985, 1988; Cas and Wright 1987; Smith 1987; White and Busby-Spera 1987; Houghton and Landis 1989; Palmer and Walton 1990; Fisher and Smith 1991; Fisher and Schmincke 1994; Smith and Landis 1995; Orton 1996; Wright 1996; Carey 2000; Mitchell 2000; Gamberi 2001; Karátson and Németh 2001; Allen *et al*. 2006; Casalbore *et al*. 2010; Carey and Schneider 2011). In these papers, a volcaniclastic apron is defined as a thick accumulation of coarse volcanic debris that fringes a volcano or a chain of volcanoes and builds outward from them; volcaniclastic aprons are typically fan shaped or are composed of coalescing fans that form a wedge. They are steep in their proximal reaches, with abundant large lithic blocks and slumps, passing smoothly into medial to distal reaches that have gentler slopes, formed of debris flow and coarse-grained pyroclastic density current deposits. For example, the 'volcanic apron' of Gran Canaria is a volcaniclastic apron (Funck *et al*. 1996), consisting of volcano-flank seismically chaotic pillow breccia and hylaoclastite and poorly stratified debris flow deposits, which pass basinward into crudely stratified slump, debris flow, and turbidity current deposits. The submarine flanks of Anahatan Volcano and Northeast Anahatan Volcano (Mariana Arc) are largely mantled with volcaniclastic aprons, which extend 5–20 km from the island of Anahatan; these have slopes decreasing from 15–25° to 5° with

distance, and their outer edge is marked by a distinct break in slope, with abyssal sediment beyond (Chadwick *et al.* 2005). Volcaniclastic aprons form in both nonmarine and marine environments, and they commonly prograde into basins with time, producing an overall upward-coarsening sequence.

The depositional model for Site U1437 must take account of the fact that it is an entirely deep-water deposit, and using the criteria above, it clearly does not represent a volcaniclastic apron. The depositional model may instead be based on analogies with the other major type of deep-water depositional system, the submarine fans and aprons of siliciclastic deep-water systems. Submarine fans and aprons are relatively coarse grained constructional features, whereas the basin plain beyond is flat and fine grained with laterally continuous deposits (Reading and Richards 1994; Stow *et al.* 1996; Richards 2009). The upper 75% of the section drilled at Site U1437 is analogous to the basin plain; it is a fine-grained, well-stratified sequence with laterally continuous layers. For this reason, we refer to it as a deep-water basinal succession, not a volcaniclastic apron.

The lower 25% of the section, in contrast, consists largely of blocky hyaloclastic deposits (unit VII, 347 m) that cooled *in situ* with very limited remobilization and thus represent near-vent deposits. It also includes lesser polymict lapilli tuffs (unit VI, 140 m) sourced from nearby volcanoes but also with rhyolite blocks locally derived from igneous unit I (within unit VI). Therefore, the lower 25% of the section is dominated by localized vent-related deposits within the deep-water basinal succession. As discussed earlier, the geochemistry of the lower 25% also differs from the upper 75% of the section.

Conclusion: surprises and questions to be addressed in shore-based investigations

Four surprises resulted from drilling at U1437 that led to questions for on-going (shore-based) investigation, to be summarized in future papers.

The first surprise is that the section is much more mud-rich than expected for an arc-proximal sedimentary succession. The section as a whole is 60% tuffaceous mudstone, with 89% in the uppermost 433 m, and with high sedimentation rates of 100–260 m/million year for the upper 1300 m. What was the source of all that mud, and how was it deposited?

The second surprise is that the grain size of the volcaniclastics is much smaller than expected for an arc-proximal sedimentary succession, composed of half ash/tuff and half fine-grained lapilli tuff. No

volcanic blocks are present in the upper 75% of the section. Yet Site U1437 lies downslope, within kilometres to tens of kilometre, of seamounts dated at 6.86–6.53 (Manji), 3.76 Ma (Meoreki), and 5.05 and 0.55 Ma (Daigo-Nishi-Aogashima Knoll) from dredged samples, as shown in Figure 7. This may indicate that most <7 Ma eruptions from the seamounts were small-volume effusions that did not produce much volcaniclastic material. Alternatively, the dredged samples represent late-stage, small volume eruptions that mantle the surfaces on the seamounts, and they were largely built before ~9 Ma.

The third surprise is that the section is much younger than predicted from seismic stratigraphy. For example, Oligocene (>23 Ma) strata were predicted at 1250 mbsf, but instead those strata are 9 Ma (Miocene).

Fourth, it was predicted that compositional divergence between arc-front and rear-arc magmas developed during a volcanic hiatus associated with opening of the backarc basin at 27–17 Ma, if it did not already exist from the time of arc inception in the Eocene (~45 Ma); however, preliminary data presented here suggest that this divergence only fully developed after ~13–14 Ma (middle Miocene). The cause is not known.

Disclosure statement

No potential conflict of interest was reported by the authors.

References

Allen, S.R., Hayward, B.W., and Mathews, E., 2006, A facies model for a submarine volcaniclastic apron: The Miocene Manukau Subgroup, New Zealand: Geological Society of America Bulletin, v. 119, no. 5–6, p. 725–742. doi:10.1130/B26066.1

Andrews, G.D.M., Schmitt, A.K., Busby, C.J., and Brown, S.R., 2015, Geochronology and geochemistry of zircons from IODP Site U1437: in the rear arc of the Izu-Bonin volcanic chain: American Geophysical Union Fall Meeting, Abstract DI13A-2627.

Arculus, R., Ishizuka, O., and Bogus, K.A., 2013, Izu-Bonin-Mariana arc origins: Continental crust formation at intraoceanic arc: Foundations, inceptions, and early evolution:

International Ocean Discovery Program Scientific Prospectus, p. 351. doi:10.2204/iodp.sp.351.2013

Arculus, R., Ishizuka, O., and Bogus, M.H. and the Expedition 351 Scientists, 2015, Proceedings of the Internaitonal Ocean Discovery Program, Volume 351 publications.iodp. org. doi:10.14379/iodp.proc.351.101.2015

Bandy, W.L., and Hilde, T.W.C., 1983, Structural features of the Bonin arc: Implications for its tectonic history: Tectonophysics, v. 99, no. 2–4, p. 331–353. doi:10.1016/0040-1951(83)90111-7

Bloomer, S.H., Taylor, B., MacLeod, C.J., Stern, R.J., Fryer, P., Hawkins, J.W., and Johnson, L., 1995, Early arc volcanism and the ophiolite problem: A perspective from drilling in the western Pacific, in Taylor, B., and Natland, J., eds., Active margins and marginal basins of the western Pacific: Geophysical Monograph, v. 88, p. 1-30. doi:10.1029/GM088p0001

Bryant, C.J., Arculus, R.J., and Eggins, S.M., 2003, The geochemical evolution of the Izu-Bonin arc system: A perspective from tephras recovered by deep-sea drilling: Geochemistry, Geophysics, Geosystems, v. 4, no. 11, p. 1094. doi:10.1029/2002GC000427

Busby-Spera, C.J., 1985, A sand-rich submarine fan in the lower Mesozoic Mineral King caldera complex, Sierra Nevada, California: Journal of Sedimentary Research, v. 55, no. 3, p. 376–391. doi:10.1306/212F86D9-2B24-11D7-8648000102C1865D

Busby-Spera, C.J., 1988, Evolution of a middle Jurassic back-arc basin, Cedros Island, Baja California: Evidence from a marine volcaniclastic apron: Geological Society of America Bulletin, v. 100, no. 2, p. 218–233. doi:10.1130/0016-7606(1988)100<0218:EOAMJB>2.3.CO;2

Busby-Spera, C.J., and White, J.D.L., 1987, Variation in peperite textures associated with differing host-sediment properties: Bulletin of Volcanology, v. 49, no. 6, p. 765–776. doi:10.1007/BF01079827

Carey, S., 1997, Influence of convective sedimentation on the formation of widespread tephra fall layers in the deep sea: Geology, v. 25, no. 9, p. 839–842. doi:10.1130/0091-7613(1997)025<0839:IOCSOT>2.3.CO;2

Carey, S., 2000, Volcaniclastic sedimentation around island arcs, in Sigurdsson, H., Houghton, B.F., McNutt, S.R., Rymer, H., and Stix, J., eds., Encyclopedia of volcanoes, San Diego: Academic Press, p. 627–642.

Carey, S., and Sigurdsson, H., 1984, A model of volcanogenic sedimentation in marginal basins, in Kokelaar, B.P., and Howells, M.F., eds., Marginal basin geology: Volcanic and associated sedimentary and tectonic processes in modern and ancient marginal basins: Geological Society Special Publication v. 16, p. 37-58. doi:10.1144/GSL.SP.1984.016.01.04

Carey, S.N., and Schneider, J.-L., 2011, Volcaniclastic processes and deposits in the deep sea, in Hüneke, H., and Mulder, T., eds., Developments in sedimentology, Volume 63: Deep-Sea Sediments, Oxford: Elsevier, p. 457–515. doi:10.1016/B978-0-444-53000-4.00007-X

Cas, R.A.F., and Wright, J.V., 1987, Volcanic successions, modern and ancient: A geological approach to processes, products and successions: London, Allen and Unwin.

Casalbore, D., Romagnoli, C., Chiocci, F., and Frezza, V., 2010, Morpho-sedimentary characteristics of the volcaniclastic apron around Stromboli volcano (Italy): Marine Geology, v. 269, no. 3–4, p. 132–148. doi:10.1016/j.margeo.2010.01.004

Chadwick, W.W., Embley, R.W., Johnsons, P.D., Merle, S.G., Ristau, S., and Bobbitt, A., 2005, The submarine flank of Anatahan volcano: Commonwealth of the Northern Mariana Islands: Journal of Volcanology and Geothermal Research, v. 146, p. 8–25.

Cosca, M.A., Arculus, R.J., Pearce, J.A., and Mitchell, J.G., 1998, 40Ar/39Ar and K-Ar geochronological age constraints for the inception and early evolution of the Izu-Bonin-Mariana arc system: The Island Arc, v. 7, no. 3, p. 579–595. doi:10.1111/j.1440-1738.1998.00211.x

Dickinson, W.R., and Hatherton, T., 1967, Andesitic volcanism and seismicity around the Pacific: Science, v. 157, no. 3790, p. 801–803. doi:10.1126/science.157.3790.801

Farquharson, G.W., Hamer, R.D., and Ineson, J.R., 1984, Proximal volcaniclastic sedimentation in a Cretaceous back-arc apron, northern Antarctic Peninsula, in Kokelaar, B.P., and Howells, M.F., eds., Marginal basin geology: Volcanic and associated sedimentary and tectonic processes in modern and ancient marginal basins: Geological Society Special Publication v. 16, p. 5-27. doi:10.1144/GSL.SP.1984.016.01.17

Fisher, R.V., 1984, Submarine volcaniclastic rocks, in Kokelaar, B.P., and Howells, M.F., eds., Marginal basin geology: Volcanic and associated sedimentary processes in modern and ancient basins, vol. 16. Springer-Verlag; p. 5–27. doi:10.1144/GSL.SP.1984.016.01.02

Fisher, R.V., and Schmincke, H.-U., 1984, Pyroclastic rocks: Berlin, Springer-Verlag. doi:10.1007/978-3-642-74864-6

Fisher, R.V., and Schmincke, H.-U., 1994, Volcaniclastic sediment transport and deposition, in Pye, K., eds., Sediment transport and depositional processes, Oxford, UK: Blackwell Scientific Publishing, p. 351–388.

Fisher, R.V., and Smith, G.A., 1991, Volcanism, tectonics and sedimentation, in Fisher, R.V., and Smith, G.A., eds., Sedimentation in volcanic settings, vol. 45. Special Publication-SEPM (Society for Sedimentary Geology; p. 1–5. doi:10.2110/pec.91.45.0001

Funck, T., Dickmann, T., Rihm, R., Krastel, S., Lykke-Andersen, H., and Schmincke, H.-U., 1996, Reflection seismic investigations in the volcaniclastic apron of Gran Canaria and implications for its volcanic evolution: Geophysical Journal International, v. 125, no. 2, p. 519–536. doi:10.1111/j.1365-246X.1996.tb00015.x

Gamberi, F., 2001, Volcanic facies associations in a modern volcaniclastic apron (Lipari and Vulcano offshore, Aeolian Island arc): Bulletin of Volcanology, v. 63, no. 4, p. 264–273. doi:10.1007/s004450100143

Gill, J.B., 1981, Minerals and rocks, Volume 16: Orogenic Andesites and Plate Tectonics: Berlin, Springer-Verlag. doi:10.1007/978-3-642-68012-0

Gill, J.B., Hiscott, R.N., and Vidal, P., 1994, Turbidite geochemistry and evolution of the Izu-Bonin arc and continents: Lithos, v. 33, no. 1–3, p. 135–168. doi:10.1016/0024-4937(94)90058-2

Hochstaedter, A., Gill, J., Peters, R., Broughton, P., Holden, P., and Taylor, B., 2001, Across-arc geochemical trends in the Izu-Bonin arc: Contributions from the subducting slab: Geochemistry, Geophysics, Geosystems, v. 2, no. 7, p. 1019. doi:10.1029/2000GC000105

Hochstaedter, A.G., Gill, J.B., Kusakabe, M., Newman, S., Pringle, M., Taylor, B., and Fryer, P., 1990a, Volcanism in the Sumisu Rift, I. Major element, volatile, and stable isotope geochemistry: Earth and Planetary Science Letters, v. 100, no. 1–3, p. 179–194. doi:10.1016/0012-821X(90)90184-Y

Hochstaedter, A.G., Gill, J.B., and Morris, J.D., 1990b, Volcanism in the Sumisu Rift, II. Subduction and non-subduction related components: Earth and Planetary Science Letters, v. 100, no. 1–3, p. 195–209. doi:10.1016/0012-821X(90)90185-Z

Hochstaedter, A.G., Gill, J.B., Taylor, B., Ishizuka, O., Yuasa, M., and Monta, S., 2000, Across-arc geochemical trends in the Izu-Bonin arc: Constraints on source composition and mantle melting: Journal of Geophysical Research: Solid Earth, v. 105, no. B1, p. 495–512. doi:10.1029/1999JB900125

Houghton, B.F., and Landis, C.A., 1989, Sedimentation and volcanism in a Permian arc-related basin, southern New Zealand: Bulletin of Volcanology, v. 51, no. 6, p. 433–450. doi:10.1007/BF01078810

Ishizuka, O., Kimura, J.-I., Li, Y.B., Stern, R.J., Reagan, M.K., Taylor, R.N., Ohara, Y., Bloomer, S.H., Ishii, T., Hargrove, U.S., III, and Haraguchi, S., 2006a, Early stages in the evolution of Izu-Bonin arc volcanism: New age, chemical, and isotopic constraints: Earth and Planetary Science Letters, v. 250, no. 1–2, p. 385–401. doi:10.1016/j.epsl.2006.08.007

Ishizuka, O., Taylor, R.N., Milton, J.A., and Nesbitt, R.W., 2003a, Fluid-mantle interaction in an intraoceanic arc: Constraints from high-precision Pb isotopes: Earth and Planetary Science Letters, v. 211, no. 3–4, p. 221–236. doi:10.1016/S0012-821X(03)00201-2

Ishizuka, O., Taylor, R.N., Milton, J.A., Nesbitt, R.W., Yuasa, M., and Sakamoto, I., 2006b, Variation in the mantle sources of the northern Izu arc with time and space—Constraints from high-precision Pb isotopes: Journal of Volcanology and Geothermal Research, v. 156, no. 3–4, p. 266–290. doi:10.1016/j.jvolgeores.2006.03.005

Ishizuka, O., Taylor, R.N., Yuasa, M., and Ohara, Y., 2011, Making and breaking an island arc: A new perspective from the Oligocene Kyushu-Palau arc, Philippine Sea: Geochemistry, Geophysics, Geosystems, v. 12, no. 5, p. Q05005. doi:10.1029/2010GC003440

Ishizuka, O., Uto, K., and Yuasa, M., 2003b, Volcanic history of the back-arc region of the Izu-Bonin (Ogasawara) arc, in Larter, R.D., and Leat, P.T., eds., Tectonic and magmatic processes, Geological Society Special Publication v. 291, p. 187-205. doi:10.1144/GSL.SP.2003.219.01.09

Ishizuka, O., Uto, K., Yuasa, M., and Hochstaedter, A.G., 1998, K-Ar ages from seamount chains in the back-arc region of the Izu-Ogasawara arc: The Island Arc, v. 7, no. 3, p. 408–421. doi:10.1111/j.1440-1738.1998.00199.x

Ishizuka, O., Yuasa, M., and Uto, K., 2002, Evidence of porphyry copper-type hydrothermal activity from a submerged remnant back-arc volcano of the Izu-Bonin arc: Implications for the volcanotectonic history of back-arc seamounts: Earth and Planetary Science Letters, v. 198, no. 3–4, p. 381–399. doi:10.1016/S0012-821X(02)00515-0

Karátson, D., and Németh, K., 2001, Lithofacies associations of an emerging volcaniclastic apron in a Miocene volcanic complex: An example from the Börzsöny Mountains, Hungary: International Journal of Earth Sciences, v. 90, no. 4, p. 776–794. doi:10.1007/s005310100193

Karig, D.E., and Moore, G.F., 1975a, Tectonic complexities in the Bonin arc system: Tectonophysics, v. 27, no. 2, p. 97–118. doi:10.1016/0040-1951(75)90101-8

Karig, D.E., and Moore, G.F., 1975b, Tectonically controlled sedimentation in marginal basins: Earth and Planetary Science Letters, v. 26, no. 2, p. 233–238. doi:10.1016/0012-821X(75)90090-4

Kodaira, S., Sato, T., Takahashi, N., Ito, A., Tamura, Y., Tatsumi, Y., and Kaneda, Y., 2007a, Seismological evidence for variable growth of crust along the Izu intraoceanic arc: Journal of Geophysical Research: Solid Earth, v. 112, no. B5, p. B05104. doi:10.1029/2006JB004593

Kodaira, S., Sato, T., Takahashi, N., Miura, S., Tamura, Y., Tatsumi, Y., and Kaneda, Y., 2007b, New seismological constraints on growth of continental crust in the Izu-Bonin intra-oceanic arc: Geology, v. 35, no. 11, p. 1031–1034. doi:10.1130/G23901A.1

Kodaira, S., Sato, T., Takahashi, N., Yamashita, M., No, T., and Kaneda, Y., 2008, Seismic imaging of a possible paleoarc in the Izu-Bonin intraoceanic arc and its implications for arc evolution processes: Geochemistry, Geophysics, Geosystems, v. 9, no. 10, p. Q10X01. doi:10.1029/2008GC002073

Konrad, K., Schmitt, A.K., Andrews, G.D., Horle, K., Brown, S.R., Koppers, A.A.P., Busby, C., and Tamura, Y., 2016, 40Ar/39Ar dating and zircon chronochemistry for the Izu-Bonin rear arc, in IODP site U1437: American Geophysical Union Fall Meeting, Abstract V13C-2853.

Kuno, H., 1959, Origin of Cenozoic petrographic provinces of Japan and surrounding areas: Bulletin of Volcanology, v. 20, no. 1, p. 37–76. doi:10.1007/BF02596571

Machida, S., and Ishii, T., 2003, Backarc volcanism along the en echelon seamounts: The Enpo Seamount chain in the northern Izu-Ogasawara arc: Geochemistry, Geophysics, Geosystems, v. 4, no. 8, p. 9006. doi:10.1029/2003GC000554

Machida, S., Ishii, T., Kimura, J.-I., Awaji, S., and Kato, Y., 2008, Petrology and geochemistry of cross-chains in the Izu-Bonin back arc: Three mantle components with contributions of hydrous liquids from a deeply subducted slab: Geochemistry, Geophysics, Geosystems, v. 9, no. 5, p. Q05002. doi:10.1029/2007GC001641

Manville, V., and Wilson, C.J.N., 2004, Vertical density currents: A review of their potential role in the deposition and interpretation of deep-sea ash layers: Journal of the Geological Society, v. 161, no. 6, p. 947–958. doi:10.1144/0016-764903-067

McPhie, J., Doyle, M., and Allen, R., 1993, Volcanic textures: A guide to the interpretation of textures in volcanic rocks: Hobart, Tasmanian Government Printing Office.

Mitchell, S.F., 2000, Facies analysis of a Cretaceous–Paleocene volcaniclastic braid-delta, in Presented at the Geological Society of Trinidad and Tobago 2000 SPE Conference and Exhibition, Port of Spain, Trinidad, 10–13 July 2000 (Paper SS03). http://archives.datapages.com/data/gstt/SS03F.PDF

Orton, G.J., 1996, Volcanic environments, in Reading, H.G., eds., Sedimentary environments: Processes, facies and stratigraphy, Oxford, UK: Blackwell Science Publishing, p. 485–573.

Palmer, B.A., and Walton, A.W., 1990, Accumulation of volcaniclastic aprons in the Mount Dutton Formation (Oligocene–Miocene), Marysvale volcanic field, Utah: Geological Society of America Bulletin, v. 102, no. 6, p.

734–748. doi:10.1130/0016-7606(1990)102<0734:AOVAIT>2.3.CO;2

Pearce, J.A., Reagan, M.K., Stern, R.J., and Petronotis, K., 2013, Izu-Bonin-Mariana fore-arc: Testing subduction initiation and ophiolite models by drilling the outer Izu-Bonin-Mariana fore arcfore-arc: International Ocean Drilling Program Scientific Prospectus, v. 352. doi:10.14379/iodp.sp.352.2013

Plank, T., 2014, The chemical composition of subducting sediments, in Rudnick, R.L., ed., Treatise on geochemistry (second edition), Volume 4: The Crust. Holland, H.D., and Turekian, K.K. (Series eds.), Oxford: Elsevier, p. 607–629. doi:10.1016/B978-0-08-095975-7.00319-3

Reading, H.G., and Richards, M., 1994, Turbidite systems in deep-water basin margins classified by grain size and feeder system: AAPG Bulletin, v. 78, no. 5, p. 792–822. http://aapgbull.geoscienceworld.org/cgi/content/abstract/78/5/792

Reagan, M.K., Ishizuka, O., Stern, R.J., Kelley, K.A., Ohara, Y., Blichert-Toft, J., Bloomer, S.H., Cash, J., Fryer, P., Hanan, B.B., Hickey-Vargas, R., Ishii, T., Kimura, J.-I., Peate, D.W., Rowe, M. C., and Woods, M., 2010, Fore-arc basalts and subduction initiation in the Izu-Bonin-Mariana system: Geochemistry, Geophysics, Geosystems, v. 11, no. 3, p. Q03X12. doi:10.1029/2009GC002871

Reagan, M.K., Pearce, J.A., and Petronotis, K., and Expedition Scientists, 2015, Izu-Bonin-Mariana Fore Arc. Proceedings of the International Ocean Discovery Program: International Ocean Discovery Program, v. 352. doi:10.14379/iodp.proc.352.2015

Richards, M.T., 2009, Deep-marine clastic systems, in Emery, D., and Myers, K., eds., Sequence stratigraphy, London: Blackwell Science Publishing, p. 178–210. doi:10.1002/9781444313710.ch9

Sample, J.C., and Karig, D.E., 1982, A volcanic production rate for the Mariana island arc: Journal of Volcanology and Geothermal Research, v. 13, no. 1–2, p. 73–82. doi:10.1016/0377-0273(82)90020-8

Smith, G.A., 1987, Sedimentology of volcanism-induced aggradation in fluvial basins: Examples from the Pacific Northwest, U.S.A., in Ethridge, F.G., Flores, R.M., and Harvey, M.D., eds., Recent developments in fluvial sedimentology, Special Publication – SEPM (Society for Sedimentary Geology) v. 39, p. 217-228. doi:10.2110/pec.87.39.0217

Smith, G.A., and Landis, C., 1995, Intra-arc basins, in Busby, C. J., and Ingersoll, R.V., eds., Tectonics of sedimentary basins, Oxford: Blackwell Science Publishing, p. 263–298.

Stern, R.J., Fouch, M.J., and Klemperer, S., 2003, An overview of the Izu-Bonin-Mariana subduction factory, in Eiler, J., eds., Inside the subduction factory: Geophysical Monograph v. 138, p. 175-122. doi:10.1029/138GM10

Stow, D.A.V., Reading, H.G., and Collinson, J.D., 1996, Deep seas, in Reading, H.G., eds., Sedimentary environments: Processes, facies and stratigraphy, Oxford, UK: Blackwell Science Publishing, p. 395–453.

Straub, S.M., 2003, The evolution of the Izu Bonin - Mariana volcanic arcs (NW Pacific) in terms of major element chemistry: Geochemistry, Geophysics, Geosystems, v. 4, no. 2, p. 1018. doi:10.1029/2002GC000357

Straub, S.M., Goldstein, S.L., Class, C., Schmidt, A., and Gomez-Tuena, A., 2010, Slab and mantle controls on the Sr–Nd–Pb–Hf isotope evolution of the post 42 Ma Izu–Bonin volcanic arc: Journal of Petrology, v. 51, no. 5, p. 993–1026. doi:10.1093/petrology/egq009

Suyehiro, K., Takahashi, N., Ariie, Y., Yokoi, Y., Hino, R., Shinohara, M., Kanazawa, T., Hirata, N., Tokuyama, H., and Taira, A., 1996, Continental crust, crustal underplating, and low-Q upper mantle beneath an oceanic island arc: Science, v. 272, no. 5260, p. 390–392. doi:10.1126/science.272.5260.390

Tamura, Y., Busby, C., and Blum, P., 2013, Izu-Bonin-Mariana Rear Arc: The missing half of the subduction factory: International Ocean Discovery Program Scientific Prospectus, p. 350. doi:10.2204/iodp.sp.350.2013

Tamura, Y., Busby, C.J., Blum, P., Guèrin, G., Andrews, G.D.M., Barker, A.K., Berger, J.L.R., Bongiolo, E.M., Bordiga, M., DeBari, S.M., Gill, J.B., Hamelin, C., Jia, J., John, E.H., Jonas, A.-S., Jutzeler, M., Kars, M.A.C., Kita, Z.A., Konrad, K., Mahoney, S.H., Martini, M., Miyazaki, T., Musgrave, R.J., Nascimento, D.B., Nichols, A.R.L., Ribeiro, J.M., Sato, T., Schindlbeck, J.C., Schmitt, A.K., Straub, S.M., Vautravers, M. J., and Yang, Y., 2015a, Expedition 350 summary, in Tamura, Y., Busby, C.J., and Blum, P., and the Expedition 350 Scientists, eds., Proceedings of the International Ocean Discovery Program, Expedition 350: Izu-Bonin-Mariana Rear Arc, College Station, TX: International Ocean Discovery Program. doi:10.14379/iodp.proc.350.101.2015

Tamura, Y., Busby, C.J., Blum, P., Guèrin, G., Andrews, G.D.M., Barker, A.K., Berger, J.L.R., Bongiolo, E.M., Bordiga, M., DeBari, S.M., Gill, J.B., Hamelin, C., Jia, J., John, E.H., Jonas, A.-S., Jutzeler, M., Kars, M.A.C., Kita, Z.A., Konrad, K., Mahoney, S.H., Martini, M., Miyazaki, T., Musgrave, R.J., Nascimento, D.B., Nichols, A.R.L., Ribeiro, J.M., Sato, T., Schindlbeck, J.C., Schmitt, A.K., Straub, S.M., Vautravers, M. J., and Yang, Y., 2015b, Expedition 350 methods, in Tamura, Y., Busby, C.J., and Blum, P., and the Expedition 350 Scientists, eds., Proceedings of the International Ocean Discovery Program, Expedition 350: Izu-Bonin-Mariana Rear Arc, College Station, TX: International Ocean Discovery Program. doi:10.14379/iodp.proc.350.102.2015

Tamura, Y., Busby, C.J., Blum, P., Guèrin, G., Andrews, G.D.M., Barker, A.K., Berger, J.L.R., Bongiolo, E.M., Bordiga, M., DeBari, S.M., Gill, J.B., Hamelin, C., Jia, J., John, E.H., Jonas, A.-S., Jutzeler, M., Kars, M.A.C., Kita, Z.A., Konrad, K., Mahoney, S.H., Martini, M., Miyazaki, T., Musgrave, R.J., Nascimento, D.B., Nichols, A.R.L., Ribeiro, J.M., Sato, T., Schindlbeck, J.C., Schmitt, A.K., Straub, S.M., Vautravers, M. J., and Yang, Y., 2015c, Site U1436, in Tamura, Y., Busby, C.J., and Blum, P., and the Expedition 350 Scientists, eds., Proceedings of the International Ocean Discovery Program, Expedition 350: Izu-Bonin-Mariana Rear Arc, College Station, TX: International Ocean Discovery Program. doi:10.14379/iodp.proc.350.103.2015

Tamura, Y., Busby, C.J., Blum, P., Guèrin, G., Andrews, G.D.M., Barker, A.K., Berger, J.L.R., Bongiolo, E.M., Bordiga, M., DeBari, S.M., Gill, J.B., Hamelin, C., Jia, J., John, E.H., Jonas, A.-S., Jutzeler, M., Kars, M.A.C., Kita, Z.A., Konrad, K., Mahoney, S.H., Martini, M., Miyazaki, T., Musgrave, R.J., Nascimento, D.B., Nichols, A.R.L., Ribeiro, J.M., Sato, T., Schindlbeck, J.C., Schmitt, A.K., Straub, S.M., Vautravers, M. J., and Yang, Y., 2015d, Site U1437, in Tamura, Y., Busby, C. J., and Blum, P., and the Expedition 350 Scientists, eds., Proceedings of the International Ocean Discovery Program, Expedition 350: Izu-Bonin-Mariana Rear Arc,

College Station, TX: International Ocean Discovery Program. doi:10.14379/iodp.proc.350.104.2015

Tamura, Y., Gill, J.B., Tollstrup, D., Kawabata, H., Shukuno, H., Chang, Q., Miyazaki, T., Takahashi, T., Hirahara, Y., Kodaira, S., Ishizuka, O., Suzuki, T., Kido, Y., Fiske, R.S., and Tatsumi, Y., 2009, Silicic magmas in the Izu-Bonin oceanic arc and implications for crustal evolution: Journal of Petrology, v. 50, no. 4, p. 685–723. doi:10.1093/petrology/egp017

Tamura, Y., Ishizuka, O., Aoike, K., Kawate, S., Kawabata, H., Chang, Q., Saito, S., Tatsumi, Y., Arima, M., Takahashi, M., Kanamaru, T., Kodaira, S., and Fiske, R.S., 2010, Missing Oligocene crust of the Izu-Bonin arc: Consumed or rejuvenated during collision?: Journal of Petrology, v. 51, no. 4, p. 823–846. doi:10.1093/petrology/egq002

Tamura, Y., and Tatsumi, Y., 2002, Remelting of an andesitic crust as a possible origin for rhyolitic magma in oceanic arcs: An example from the Izu-Bonin arc: Journal of Petrology, v. 43, no. 6, p. 1029–1047. doi:10.1093/petrology/43.6.1029

Tamura, Y., Tatsumi, Y., Zhao, D., Kido, Y., and Shukuno, H., 2002, Hot fingers in the mantle wedge: New insights into magma genesis in subduction zones: Earth and Planetary Science Letters, v. 197, no. 1–2, p. 105–116. doi:10.1016/S0012-821X(02)00465-X

Taylor, B., 1992, Rifting and the volcanic-tectonic evolution of the Izu-Bonin-Mariana arc, in Taylor, B., Fujioka, K., et al., eds., Proceedings of the Ocean Drilling Program, scientific results, 126, College Station, TX: Ocean Drilling Program, p. 627–651. doi:10.2973/odp.proc.sr.126.163.1992

Taylor, B., Fujioka, K., et al., 1990, Proceedings of the Ocean Drilling Program, initial reports, Volume 126: College Station, TX, Ocean Drilling Program.

Tollstrup, D., Gill, J., Kent, A., Prinkey, D., Williams, R., Tamura, Y., and Ishizuka, O., 2010, Across-arc geochemical trends in the Izu-Bonin arc: Contributions from the subducting slab, revisited: Geochemistry, Geophysics, Geosystems, v. 11, no. 1, p. Q01X10. doi:10.1029/2009GC002847

Wentworth, C.K., 1922, A scale of grade abd class terms for clastic sediments: Journal of Geology, v. 30, no. 4, p. 377–392. doi:10.1086/622910

White, J. D. L., and Busby-Spera, C. J., 1987, Deep marine arc apron deposits and syndepositional magmatism in the Alisitos Group at Punta Cono, Baja California, Mexico: Sedimentology, v. 34, no. 5, p. 911-927 doi:10.1111/j.1365-3091.1987.tb00812.x

Wright, I.C., 1996, Volcaniclastic processes on modern submarine arc stratovolcanoes: Sidescan and photographic evidence from the Rumble IV and V volcanoes, southern Kermadec Arc (SW Pacific): Marine Geology, v. 136, no. 1–2, p. 21–39. doi:10.1016/S0025-3227(96)00054-0

Yamashita, M., Takahashi, N., Tamura, Y., Miura, S., and Kodaira, S., 2017, Seismic imaging for an ocean drilling site survey and its verification in the Izu rear arc: Exploration Geophysics. doi:10.1071/EG16142

Yamazaki, T., and Stern, R.J., 1997, Topography and magnetic vector anomalies in the Mariana Trough: JAMSTEC Deep Sea Research, v. 13, p. 31–45.

Yamazaki, T., and Yuasa, M., 1998, Possible Miocene rifting of the Izu–Ogasawara (Bonin) arc deduced from magnetic anomalies: The Island Arc, v. 7, no. 3, p. 374–382. doi:10.1111/j.1440-1738.1998.00196.x